Article

Neuronal substance P drives metastasis through an extracellular RNA–TLR7 axis

https://doi.org/10.1038/s41586-024-07767-5

Received: 19 January 2023

Accepted: 28 June 2024

Published online: 7 August 2024

Check for updates

Veena Padmanaban[1], Isabel Keller[1], Ethan S. Seltzer[1], Benjamin N. Ostendorf[1,2,3], Zachary Kerner[4] & Sohail F. Tavazoie[1]✉

Tumour innervation is associated with worse patient outcomes in multiple cancers[1,2], which suggests that it may regulate metastasis. Here we observed that highly metastatic mouse mammary tumours acquired more innervation than did less-metastatic tumours. This enhanced innervation was driven by expression of the axon-guidance molecule SLIT2 in tumour vasculature. Breast cancer cells induced spontaneous calcium activity in sensory neurons and elicited release of the neuropeptide substance P (SP). Using three-dimensional co-cultures and in vivo models, we found that neuronal SP promoted breast tumour growth, invasion and metastasis. Moreover, patient tumours with elevated SP exhibited enhanced lymph node metastatic spread. SP acted on tumoral tachykinin receptors (TACR1) to drive death of a small population of TACR1^{high} cancer cells. Single-stranded RNAs (ssRNAs) released from dying cells acted on neighbouring tumoural Toll-like receptor 7 (TLR7) to non-canonically activate a prometastatic gene expression program. This SP- and ssRNA-induced *Tlr7* gene expression signature was associated with reduced breast cancer survival outcomes. Therapeutic targeting of this neuro–cancer axis with the TACR1 antagonist aprepitant, an approved anti-nausea drug, suppressed breast cancer growth and metastasis in multiple models. Our findings reveal that tumour-induced hyperactivation of sensory neurons regulates multiple aspects of metastatic progression in breast cancer through a therapeutically targetable neuropeptide/extracellular ssRNA sensing axis.

Nerve fibres have been detected within malignant tissues for decades[3]. Most solid tumours are innervated by the peripheral nervous system, receiving input from autonomic (sympathetic and parasympathetic) and/or sensory nerves. Primary tumours have been shown to secrete neurotrophic factors, including members of the neurotrophin family[4] or axon-guidance molecules[5] as a means of recruiting such innervation. However, the involvement of other stromal cells in regulating tumour innervation is unclear. Tumour innervation has been increasingly implicated in experimental tumorigenesis. Glioma cells form functional synapses with neurons that promote tumour growth[6–8]. The autonomic nervous system has been shown to promote initiation of gastric[9] and prostate[10] tumours. Immunomodulatory roles have recently been reported for autonomic and sensory nerves in melanoma[11,12]. Healthy breast tissue receives abundant sensory innervation[13,14], and there is pathological evidence of breast tumour innervation[2]. However, the role of sensory innervation in breast cancer metastasis remains poorly understood. Here we used three-dimensional (3D) co-cultures and genetic and in vivo metastasis assays to define an intricate paracrine mechanism through which sensory nerves act directly on cancer cells to drive breast cancer metastasis.

Tumour endothelium regulates innervation

We recently identified that SLIT2, an axon-guidance molecule, was expressed in the endothelium of metastatic tumours[15]. Consistent with this, we observed that SLIT2 was overexpressed in the endothelium of highly metastatic breast tumours (4T1, EO771 LM2, HCC1806 LM2) relative to isogenic, poorly metastatic tumours (Extended Data Fig. 1a,b). Given its established role in axon guidance[16], we hypothesized that endothelial-derived SLIT2 may regulate innervation of primary breast tumours. To test this, we performed orthotopic transplantations of 4T1 breast cancer cells into an inducible knockout model (*Cdh5(PAC)-creERT2*) in which tamoxifen was used to drive endothelial-specific deletion of *Slit2*. The control mice had *Slit2*-floxed alleles but were Cre-negative and received equal amounts of tamoxifen. Loss of endothelial-derived SLIT2 strongly reduced tumoural innervation, including a significant reduction in sensory innervation (Extended Data Fig. 1c,d). By contrast, loss of SLIT2 in the tumour compartment did not alter tumour innervation (Extended Data Fig. 1e). These data implicate SLIT2 originating from the tumour vasculature as an upstream driver of breast tumour innervation.

[1]Laboratory of Systems Cancer Biology, The Rockefeller University, New York, NY, USA. [2]Department of Hematology, Oncology, and Tumor Immunology and Berlin Institute of Health, Charité-Universitätsmedizin Berlin, Berlin, Germany. [3]Berlin Institute for Medical Systems Biology, Max Delbrück Center for Molecular Medicine, Berlin, Germany. [4]Laboratory of Mucosal Immunology, The Rockefeller University, New York, NY, USA. ✉e-mail: sohail.tavazoie@rockefeller.edu

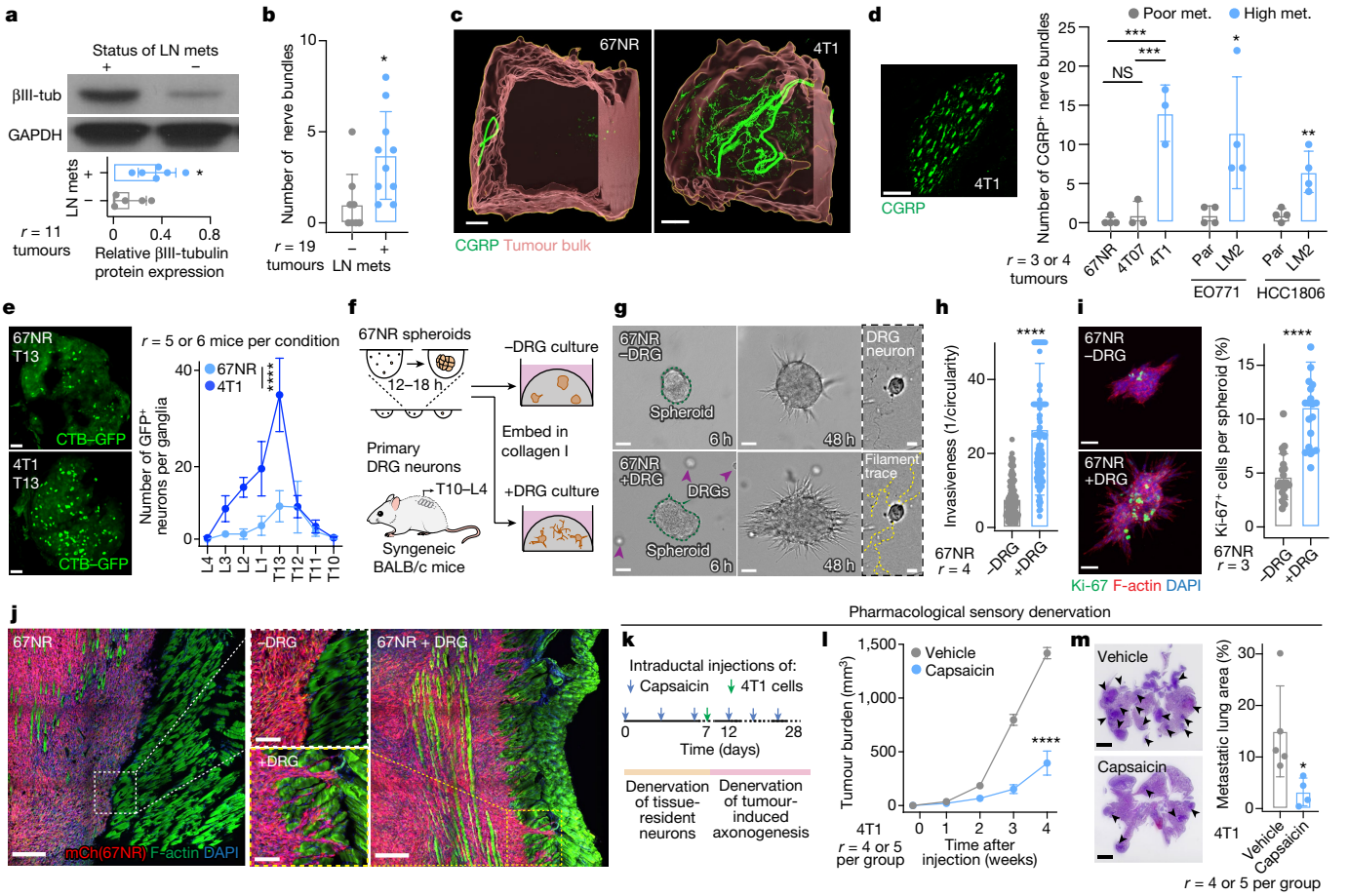

Fig. 1 | Sensory neurons promote invasion, proliferation and metastasis in breast cancer. a,**b**, Breast tumours from patients with lymph node spread express higher βIII-tubulin (βIII-tub) compared with those with localized disease, for cohort 1 (**a**; bulk protein sample tumour analysis; $r = 11$ tumours; $^{*}P = 0.0329$) and cohort 2 (**b**; FFPE sample tumour analysis; $r = 19$ tumours; $^{*}P = 0.0119$). Statistical analysis was performed using Student's *t*-test. Data are mean ± s.d. βIII-tubulin molecular mass, 50 kDa. Mets, metastases. **c**, CGRP^{+} sensory innervation in poorly (67NR) or highly (4T1) metastatic optically cleared mammary tumours. $r = 3$ tumours per group. **d**, Representative CGRP^{+} sensory nerve bundle (left), and CGRP^{+} innervation in highly metastatic primary tumours relative to corresponding isogenic poorly metastatic tumours (right). Par, parental. $^{***}P = 0.0002$ (67NR versus 4T1), $^{***}P = 0.0003$ (4T07 versus 4T1), NS, $P = 0.6636$ (67NR versus 4T07), one-way analysis of variance (ANOVA); $^{*}P = 0.0272$ (EO771, Par versus LM2), $^{**}P = 0.0073$ (HCC1806, Par versus LM2), Mann–Whitney *U*-test. Data are mean ± s.d. **e**, Retrograde tracing of DRG neurons innervating 67NR and 4T1 tumours using GFP-tagged cholera toxin β (CTB–GFP). $^{****}P < 0.0001$, Student's *t*-test of AUC. Data are mean ± s.e.m. **f**–**i**, Co-culture of 67NR cancer cell spheroids and DRG neurons isolated from syngeneic mice in 3D collagen I. **f**, Schematic of the 3D co-culture assay. **g**, Time series of 67NR cancer cell spheroids and DRG neurons. **h**,**i**, Quantification of spheroid invasion (**h**) and proliferation (**i**). $^{****}P < 0.0001$, Mann–Whitney *U*-test. Data are mean ± s.d. **j**, Representative tile scans of primary tumours arising from mCh^{+} 67NR cancer cells transplanted with or without DRG neurons. Insets: magnifications of the tumour–stroma border. Quantification is shown in Extended Data Fig. 3e. **k**–**m**, Sensory-nerve-specific denervation of 4T1 mammary tumours. **k**, Schematic. **l**, Tumour growth. $^{****}P < 0.0001$, Student's *t*-test. Data are mean ± s.e.m. **m**, The metastatic area was quantified on the basis of haematoxylin and eosin (H&E) staining. $^{*}P = 0.0385$, Student's *t*-test. Data are mean ± s.d. Scale bars, 250 µm (**j** (left and right)), 200 µm (**c** and **m**), 100 µm (**e** and **j** (middle)), 50 µm (**d**, **g** (left and middle) and **i**) and 10 µm (**g** (right)). The numbers of independent biological replicates (*r*) are indicated on the plots.

Innervation predicts metastatic ability

Our previous research established that endothelial-derived SLIT2 is a driver of metastasis. Given its ability to regulate tumour innervation, we hypothesized that innervation may regulate metastatic progression. In a survey of publicly available patient data, we observed that breast tumours expressing higher levels of pan-neuronal markers (βIII-tubulin or PGP9.5) exhibited higher rates of metastatic recurrence (Extended Data Fig. 1f). In mouse models, immunofluorescence staining and western blot analysis of βIII-tubulin revealed that highly metastatic breast tumours (4T1, EO771 LM2, HCC1806 LM2) were more innervated than their respective less metastatic isogenic tumours (67NR/4T07, EO771, HCC1806 respectively) (Extended Data Fig. 1g,h). Importantly, βIII-tubulin expression arose from the stromal compartment, consistent with its neuronal expression (Extended Data Fig. 1h). Metastatic mammary tumours at distant organ sites were also innervated (Extended Data Fig. 1i). Moreover, across the two independent patient cohorts that we analysed with a total of 30 breast tumours, increased innervation was associated with increased lymph node dissemination (Fig. 1a,b). Collectively, these findings reveal that the extent of tumoural innervation correlates with metastatic propensity.

To identify the source of peripheral innervation for breast tumours, GFP-tagged cholera-toxin β (CTB–GFP) was injected intraductally to retrogradely label neurons innervating the abdominal mammary glands of mice (Extended Data Fig. 1j). We identified dorsal root ganglia (DRG; T10–L4) sensory neurons as a predominant source of innervation for these mammary glands (Extended Data Fig. 1j,k). Importantly, we also observed abundant sensory innervation marked by calcitonin gene-related peptide (CGRP) in syngeneic (4T1 and EO771)

and genetically initiated (MMTV-PyMT and C3(1)-TAg) mouse breast cancer models, a patient-derived xenograft (PDX) model of HER2$^+$ breast cancer and three independent primary human breast tumours (Extended Data Fig. 1l). Further supporting sensory innervation of metastatic breast cancer, we observed a significantly higher degree of sensory innervation in optically cleared 4T1 tumours relative to isogenic poorly metastatic 67NR tumours (Fig. 1c). Immunofluorescence-based quantification of CGRP$^+$ nerve bundles revealed increased sensory innervation in highly metastatic tumours relative to isogenic, poorly metastatic tumours (Fig. 1d). Moreover, intratumoural nerve-tracing using CTB–GFP uncovered a far greater number of neurons within DRG innervating highly metastatic 4T1 tumours than within those innervating 67NR tumours (Fig. 1e). These findings reveal that sensory innervation is enhanced in breast tumours with higher metastatic propensity.

Sensory innervation drives metastasis

To determine whether sensory neurons affect metastatic phenotypes, we developed a 3D co-culture system comprising 67NR (poorly metastatic) cancer cell spheroids and primary sensory neurons dissected from the DRGs of syngeneic naive mice (Fig. 1f). Spheroids and neurons were embedded in 3D collagen I, a protein that is highly enriched in breast cancer stroma[17]. During the culture, DRG neurons cultured with cancer cells exhibited enhanced viability relative to those that were cultured alone (Extended Data Fig. 2a), and extended axons into the surrounding matrix (Fig. 1g and Extended Data Fig. 2b). After co-culture with DRG neurons, 67NR breast cancer spheroids exhibited significantly more invasion (Fig. 1g,h and Extended Data Fig. 2c) and proliferation (Fig. 1i). Consistent with these in vitro findings, cancer cells adjacent to nerve bundles in 4T1 primary tumours were more proliferative than cancer cells from a distant region of the same tumour (Extended Data Fig. 2d). DRG neurons enhanced the colony-forming ability of 67NR breast cancer cells within Matrigel in a cell-dose-dependent manner (Extended Data Fig. 2e,f). DRGs similarly increased the invasiveness and colony-formation ability of MMTV-PyMT-derived organoids and cancer cell clusters, respectively (Extended Data Fig. 2g–i). We next investigated the effect of DRGs on primary human tumour organoids; organoids were isolated from breast tumours of four distinct patients (three of four, ER$^+$PR$^+$HER2$^-$; one of four, ER$^+$PR$^+$HER2$^+$; Extended Data Fig. 2m) and co-cultured with mouse DRG neurons (Extended Data Fig. 2j). Consistent with our findings in mouse models, DRG neurons strongly increased invasion and proliferation of organoids from all four human tumours (Extended Data Fig. 2k,l). These findings reveal that DRG neurons enhance the proliferative and invasive phenotypes of mouse and human breast cancer cells in vitro.

We next assessed the effect of sensory innervation on breast cancer metastasis in vivo. To do this, we sought to experimentally enhance innervation of poorly metastatic 67NR tumours and conversely to reduce innervation of highly metastatic 4T1 tumours. We first co-transplanted a small number of DRG neurons along with mCherry-labelled 67NR cancer cells into syngeneic BALB/cJ hosts (Extended Data Fig. 3a). Tumoural mCherry expression enabled us to track cancer cells within non-fluorescent hosts as they progressed through the metastatic cascade. Consistent with neuronal viability and functionality after co-injection with cancer cells in vivo, we observed a significant increase in the extent of sensory innervation (Extended Data Fig. 3b) and neurotransmitter expression in these tumours (Extended Data Fig. 3c). Importantly, co-transplantation with sensory neurons significantly enhanced the growth of 67NR primary tumours (Extended Data Fig. 3d) in a neuronal-cell-dose-dependent manner (Extended Data Fig. 3i). DRGs significantly promoted the collective invasion of 67NR cancer cells into the surrounding muscle (Fig. 1j and Extended Data Fig. 3e). It is widely believed that 67NR cancer cells fail to metastasize due to their inability to intravasate[18]. However, the use of a fluorescent reporter and imaging at the single-cell resolution revealed the presence of hundreds of 67NR cancer cells within the lungs of mice (Extended Data Fig. 3f). The vast majority of these cells were associated with the lung endothelium, consistent with metastatic failure due to impaired extravasation (Extended Data Fig. 3f). A minority of 67NR cells had exited the lung endothelium to form micrometastases. This contrasted with isogeneic 4T07 cells, which efficiently formed micrometastases, and 4T1 cells, which efficiently formed macrometastases[18]. Mice that were co-transplanted with 67NR cells and DRGs had a significantly higher number of circulating mCherry$^+$ tumour cells and micrometastases (Extended Data Fig. 3g,h, respectively). Moreover, we co-injected 67NR cancer cells with DRG neurons into the tail veins of mice (Extended Data Fig. 4a) and observed neuronal cell bodies within the lung epithelium, consistent with neuronal viability after injection in vivo (Extended Data Fig. 4b). We also observed that DRG neurons significantly enhanced metastatic colonization by 67NR cancer cells in this experimental metastasis assay (Extended Data Fig. 4c). Consistently, we also observed enhanced tumour growth and micrometastases in co-transplantation experiments performed with EO771 breast cancer cells (Extended Data Fig. 4d–f). These findings reveal that DRG neurons are sufficient to enhance the metastatic capacity of breast cancer cells in co-transplantation experiments in vivo.

We next performed sensory-specific denervation of 4T1 tumours using capsaicin, a TRPV1 agonist and neurotoxin that degenerates sensory nerves. We first injected capsaicin into the mammary ductal tree to remove tissue-resident sensory innervation, then intraductally injected 4T1 cancer cells while continuing to administer capsaicin to maintain a sustained denervated state (Fig. 1k). By performing capsaicin injections intraductally, we restricted its effects to the mammary ductal epithelium. Immunofluorescence analysis confirmed successful denervation of sensory nerves within the ipsilateral mammary gland (Extended Data Fig. 5a,b). We identified that sensory-specific denervation greatly reduced tumour growth (Fig. 1l) and suppressed the number of macrometastases (quantified in mice bearing size-matched primary tumours; Fig. 1m). Importantly, capsaicin had no effect on the invasiveness or proliferation of 4T1 cancer cells in vitro, consistent with the impact of capsaicin on these phenotypes occurring through its effects on neurons, rather than on tumour cells (Extended Data Fig. 5c,d). To further control for possible confounding effects of TRPV1 agonism in immune cells[19], we repeated these experiments in immunodeficient NOD-SCID gamma (NSG) mice bearing 4T1 tumours and observed similar anti-tumour effects of capsaicin (Extended Data Fig. 5e,f). Collectively, these findings demonstrate the requirement for sensory innervation in breast cancer progression and metastasis.

Neuronal SP drives metastasis

Cancer cells are known to migrate along nerves in a process called perineural invasion[20], requiring physical contact. However, in our co-culture models, we did not detect physical interactions between neurons and cancer cells (Extended Data Fig. 2b). We therefore hypothesized that DRG neurons may mediate pro-metastatic effects through secreted molecules. To test this, we collected conditioned medium from 67NR tumour–DRG co-cultures (DRG-CM) (Fig. 2a). We used conditioned medium from 67NR-tumour-only cultures as a control (tumour-CM). Treatment of 67NR cancer cells with DRG-CM phenocopied the invasion and proliferation effects of DRG neurons (Fig. 2b,c), consistent with a secreted mediator.

Sensory DRG neurons secrete neuropeptides that stimulate various biological processes. We tested the ability of three common DRG-secreted neuropeptides[21]—CGRP, SP and galanin—to promote invasion of 67NR spheroids into collagen I. We found that SP and galanin significantly increased 67NR spheroid invasion and proliferation (Extended Data Fig. 6a–c), with SP exerting the largest magnitude effect, while CGRP exhibited a modest effect (Fig. 2d and Extended Data Fig. 6b). Importantly, DRG-CM contained higher levels of SP than

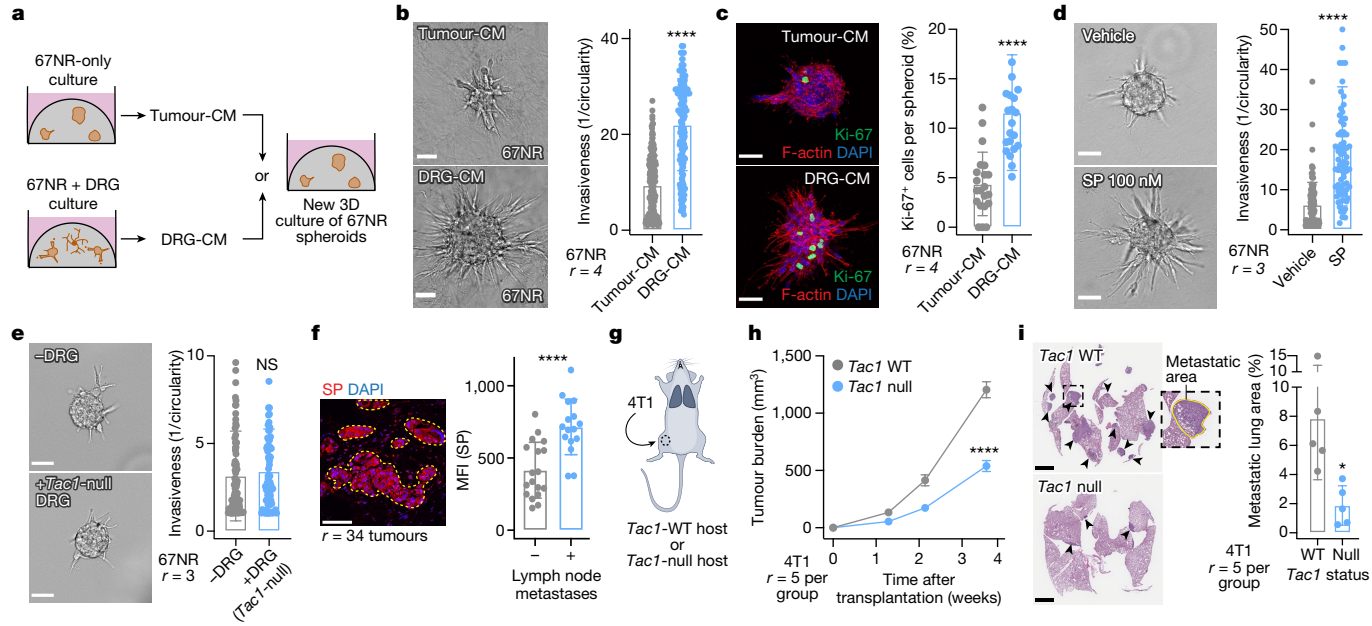

Fig. 2 | Neuronal SP promotes breast cancer metastasis. a–**c**, Tumour-CM was isolated from a 3D culture of 67NR spheroids. DRG-CM was isolated from a 3D co-culture of 67NR spheroids and DRG neurons. **a**, Schematic of the 3D DRG-conditioned medium assay. **b**,**c**, Quantification of spheroid invasion (**b**) and proliferation (**c**). ****$P < 0.0001$, Mann–Whitney *U*-test. Data are mean ± s.d. **d**, Invasion quantification of 67NR spheroids cultured with or without SP. ****$P < 0.0001$, Mann–Whitney *U*-test. Data are mean ± s.d. **e**, Invasion quantification of 67NR spheroids co-cultured with or without DRG neurons isolated from *Tac1*-null mice. NS, $P = 0.3070$, Mann–Whitney *U*-test. Data are mean ± s.d. **f**, A primary human breast tumour immunostained for SP, with the highlighted tumour region of interest (ROI) used for mean fluorescence intensity (MFI) measurements (left), and MFI of SP in breast tumours of patients with lymphatic spread versus those with localized disease (right). ****$P < 0.0001$, Student's *t*-test. Data are mean ± s.d. **g**–**i**, Orthotopic transplantation of 4T1 cells into the abdominal mammary glands of *Tac1*-WT and *Tac1*-null host mice. **g**, Schematic. **h**, Tumour growth. ****$P < 0.0001$, Student's *t*-test. Data are mean ± s.e.m. **i**, The metastatic area was quantified on the basis of H&E staining. *$P = 0.0165$, Student's *t*-test. Data are mean ± s.d. Scale bars, 200 µm (**i**) and 50 µm (**b**–**f**).

tumour-CM (Extended Data Fig. 6d). As an orthogonal approach, we performed a co-culture containing SP-deficient DRG neurons isolated from *Tac1*-null mice (encoding the precursor protein for SP). We found that *Tac1*$^{-/-}$ DRG neurons had no impact on the invasiveness of 67NR spheroids (Fig. 2e), demonstrating that the neuropeptide SP is required for the pro-invasive effects of DRG neurons on breast cancer cells.

Mice bearing highly metastatic 4T1 tumours exhibited higher SP expression in the tumour compartment and the plasma (Extended Data Fig. 6e,f) relative to mice with poorly metastatic 67NR tumours. This SP expression was innervation-dependent, as intraductal treatment of 4T1 tumours with capsaicin, a sensory neurotoxin, significantly reduced the tumoural SP levels (Extended Data Fig. 6g). Importantly, SP expression was higher in primary tumours of patients with lymph node metastases relative to those with localized disease (Fig. 2f). Inhibition of extracellular SP, through intraductal administration of an anti-SP neutralizing antibody (Extended Data Fig. 6h,i), strongly reduced tumour growth and metastasis (quantified in mice bearing size-matched primary tumours; Extended Data Fig. 6j,k). Notably, mice lacking host-derived SP (*Tac1*-null) exhibited significantly reduced orthotopic tumour growth and metastasis across multiple syngenetic breast cancer models (Fig. 2g–i and Extended Data Fig. 6l–o). These data identify neuronal SP as a driver of breast tumour growth and metastasis.

The biological activity of SP is mediated through tachykinin receptor 1 (TACR1 or NK1R)[21]. To determine whether SP mediates metastasis through tumoural TACR1, we used lentiviral short hairpin RNA (shRNA)-mediated silencing to deplete *Tacr1* in 4T1 cancer cells (Extended Data Fig. 6p). *Tacr1* depletion significantly reduced 4T1 spheroid invasion and proliferation in vitro (Extended Data Fig. 6q,r) and 4T1 tumour growth and metastasis (quantified in mice bearing size-matched primary tumours; Extended Data Fig. 6s–u) in vivo.

SP causes ssRNA release from cancer cells

We observed that conditioned medium from DRG neurons alone was not sufficient to increase the invasiveness of 67NR spheroids (Extended Data Fig. 7a,b) and contained less SP than conditioned medium from the 67NR + DRG co-culture described above (DRG-CM) (Extended Data Fig. 6d). Release of SP from DRG neurons is triggered by an increase in intracellular calcium[22]. This suggests that exposure to cancer cells may affect the calcium activity of DRG neurons. To test this hypothesis, we quantified calcium levels with the Fluo-4 calcium dye (Fig. 3a). As previously reported[23], DRG neurons cultured in isolation showed minimal change in calcium levels (Fig. 3b and Extended Data Fig. 7c). By contrast, when cultured with cancer cells, DRG neurons exhibited spontaneous calcium spikes (Fig. 3b and Extended Data Fig. 7c). Consistently, we observed increased SP release from DRG neurons cultured with tumour-CM (Extended Data Fig. 6d). Furthermore, DRG neurons were unable to drive invasiveness of cancer cell spheroids after treatment with tetrodotoxin, a sodium channel blocker that inhibits action potentials (Extended Data Fig. 7d). These findings reveal a bidirectional cross-talk between cancer cells and sensory neurons, whereby cancer cells enhance sensory neuron activity, driving SP release, which then acts on tumoural TACR1 to drive metastasis.

To systematically dissect the molecular basis through which SP (within DRG-CM) drives metastasis, we treated DRG-CM with DNase, RNase A or heat inactivation, which degrades proteins. Treatment of DRG-CM with RNase A significantly impaired the ability of DRG-CM to promote invasion of 67NR spheroids, but treatment with DNase or heat inactivation did not (Fig. 3c and Extended Data Fig. 7e). Using RNases specific for single-stranded RNA (ssRNA, RNase T1 (ref. 24)) or double-stranded RNA (dsRNA, RNase III[25]), we implicated ssRNAs

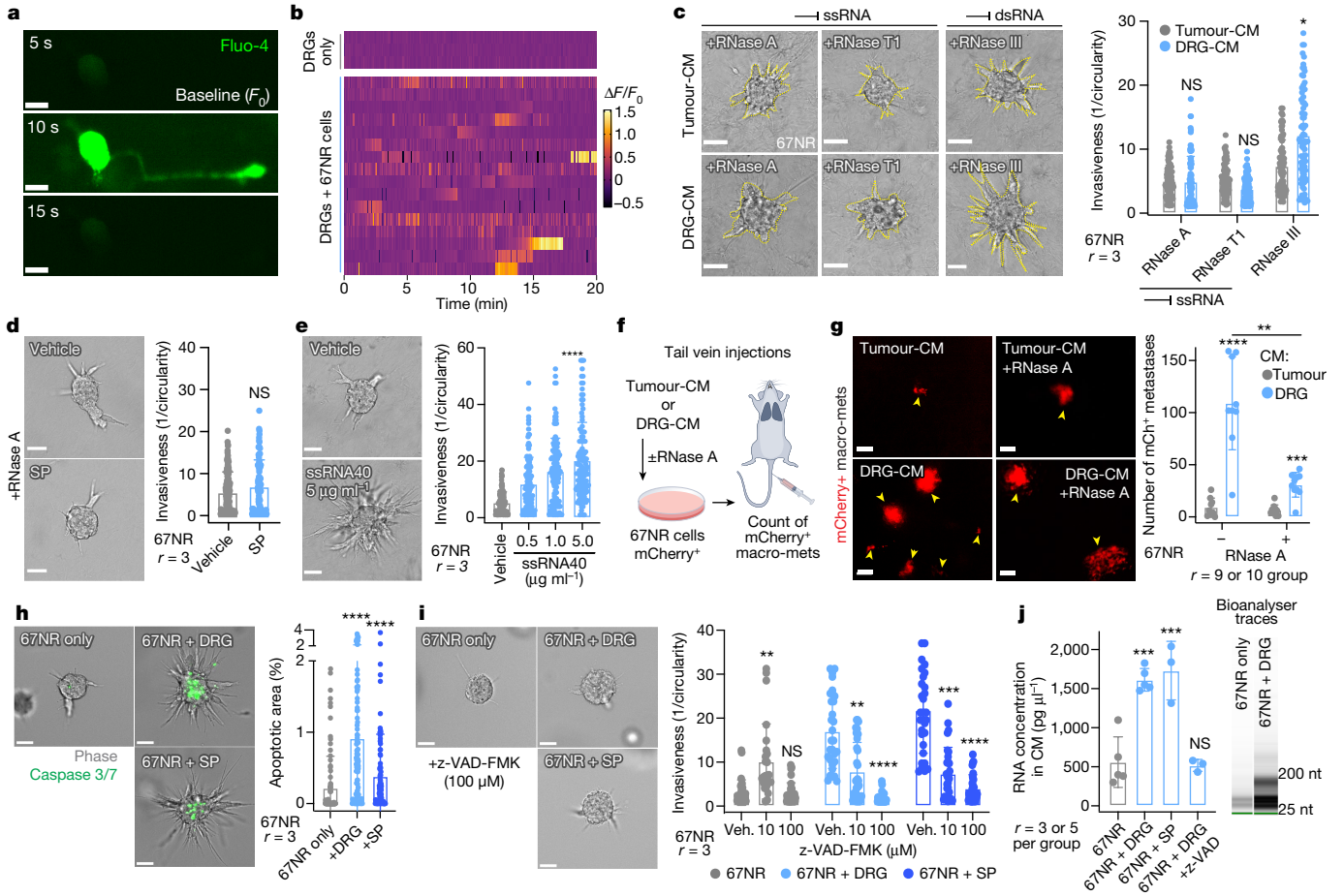

Fig. 3 | Neuronal SP promotes the release of metastatic ssRNAs from cancer cells. a, Time series of a DRG neuron co-cultured with 67NR cancer cells in the presence of the calcium dye Fluo-4. **b**, Spontaneous calcium events ($\Delta F/F_0$) in DRG neurons that were cultured with or without 67NR cancer cells. **c**, 67NR spheroids were cultured in tumour-CM or DRG-CM in the presence of either ssRNA- or dsRNA-specific RNases: representative images (left), and invasion quantification (right). NS, $P > 0.9999$, $^*P = 0.0215$, Kruskal–Wallis test. Data are mean ± s.d. **d**, Invasion quantification of 67NR spheroids that were cultured with SP and RNase A. Vehicle-treated 67NR spheroids (with or without RNase A) are plotted in Extended Data Fig. 6b, as the experiments were conducted together. NS, $P = 0.2416$, Mann–Whitney U-test. Data are mean ± s.d. **e**, Invasion quantification of 67NR spheroids that were cultured with an ssRNA mimetic. $^{****}P < 0.0001$, Kruskal–Wallis test. Data are mean ± s.d. **f**,**g**, mCherry$^+$ 67NR cancer cells were pretreated with tumour-CM or DRG-CM with or without RNase A before tail-vein injection into syngeneic hosts. **f**, Schematic. **g**, Quantification of mCherry$^+$ metastases (yellow arrowheads). $^{****}P < 0.0001$, $^{***}P = 0.0005$, $^{**}P = 0.0015$, Mann–Whitney U-tests. Data are mean ± s.d. **h**, The percentage of apoptotic area within 67NR cancer cell spheroids when cultured alone, with DRG neurons or with SP. $^{****}P < 0.0001$, Kruskal–Wallis test. Data are mean ± s.d. **i**, Invasion quantification of 67NR spheroids cultured alone, with DRG neurons or with SP, all in the presence of z-VAD-FMK, a pan-caspase inhibitor. Veh., vehicle. $^{**}P = 0.0056$, NS, $P > 0.9999$ (67NR only); $^{**}P = 0.0083$, $^{****}P < 0.0001$ (67NR + DRG); $^{***}P = 0.0004$, $^{****}P < 0.0001$ (67NR + SP group), Kruskal–Wallis tests. **j**, The RNA concentration within conditioned medium (CM) of the 67NR only, 67NR + DRG (with or without z-VAD-FMK) and 67NR + SP cultures. Extracellular RNA species detected are <200 nucleotides. $^{***}P = 0.0002$, NS, $P = 0.8248$, ANOVA. Data are mean ± s.d. Scale bars, 200 µm (**g**), 50 µm (**c**–**e**, **h** and **i**) and 15 µm (**a**).

as mediators of the pro-invasive effects of DRG-CM on breast cancer cells (Fig. 3c and Extended Data Fig. 7f).

We next sought to determine whether SP and ssRNAs signal through a common pathway that drives breast cancer metastasis. We observed that treatment of 67NR spheroids with SP in the presence of RNase A completely abolished the invasion-promoting effects of SP (Fig. 3d) but did not alter the effects of CGRP or galanin (Extended Data Fig. 6b). As the above experiments were performed using exogenously added SP and in the absence of sensory neurons, we propose a model in which sensory neurons secrete SP, which in turn promotes the release of ssRNA molecules from breast cancer cells that drive invasion and proliferation.

Cancer cell dissemination is associated with increased levels of circulating nucleic acids[26] and decreased nuclease activity in the plasma of patients with cancer[27]. The use of RNases as anti-tumour agents dates to the 1950s, often with contradictory effects[28,29]. To define the role of ssRNA in breast cancer metastasis, we treated 67NR spheroids with the ssRNA mimetic ssRNA40. Treatment with ssRNA40 significantly increased spheroid invasion and proliferation, but treatment with the dsRNA mimetic poly(I:C) did not (Fig. 3e and Extended Data Fig. 7g,h). Moreover, intraductal injections of two independently generated recombinant RNase A enzymes significantly impaired tumour growth and metastasis of 4T1 cancer cells without any observed effect on dsRNA levels (Extended Data Fig. 7 i–l).

Our in vitro studies revealed ssRNAs within DRG-CM as promoters of tumour invasion. To assess the impact of DRG-CM on metastasis in vivo, we pretreated 67NR cancer cells with DRG-CM or tumour-CM for 2 days before tail-vein injection (Fig. 3f). Pretreatment with DRG-CM was sufficient to confer metastasis-forming ability onto the poorly metastatic 67NR cells, demonstrated by the formation of hundreds of macrometastases (Fig. 3g). 67NR cancer cells that were pretreated with DRG-CM also formed significantly more metastases to the lungs, liver, brain and ovaries after intracardiac injection (Extended Data Fig. 7m–o).

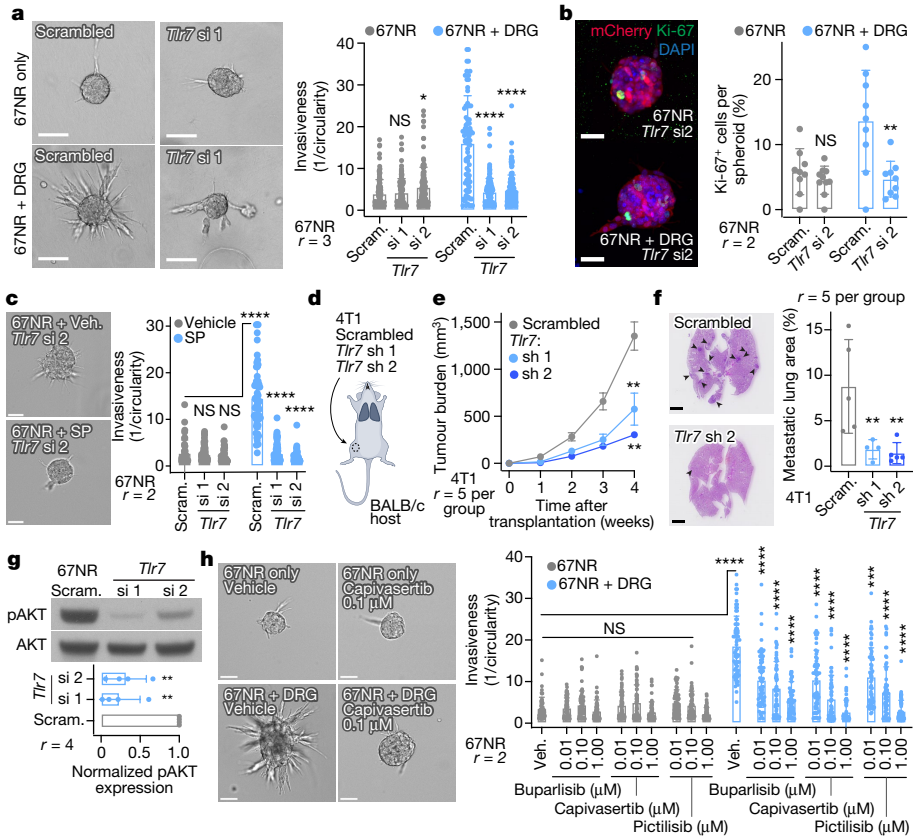

Fig. 4 | Sensory neurons signal through tumoural TLR7 to promote metastasis. a,**b**, 67NR cancer cell spheroids depleted for TLR7 and cultured with or without DRG neurons. **a**, Invasion quantification. NS, $P = 0.5787$, $^{*}P = 0.031$, $^{****}P < 0.0001$, ANOVA. **b**, Proliferation quantification. NS, $P = 0.8751$, $^{**}P = 0.0048$, Student's t-test. Data are mean ± s.d. **c**, Invasion quantification of 67NR cancer cell spheroids depleted for TLR7 and cultured with or without SP. NS, $P = 0.07$ (scrambled (scram.) versus short interfering RNA (siRNA) 1 (si 1)) and 0.926 (scrambled versus siRNA 2), $^{****}P < 0.0001$, Kruskal–Wallis test. Data are mean ± s.d. **d**–**f**, Orthotopic transplantation of 4T1 cancer cells depleted for TLR7. **d**, Schematic of the orthotopic transplantation. **e**, Tumour growth. $^{**}P = 0.0070$ (scrambled versus sh 1), $^{**}P = 0.0017$ (scrambled versus sh 2), ANOVA. Data are mean ± s.e.m. **f**, The metastatic area was quantified on the basis of H&E staining. $^{**}P = 0.0086$ (scrambled versus sh 1), $^{**}P = 0.0085$ (scrambled versus sh 2), ANOVA. Data are mean ± s.d. **g**, Western blot analysis of phosphorylated and total AKT levels in 67NR cancer cells depleted of *Tlr7*. $^{**}P = 0.0013$ (scrambled versus siRNA 1), $^{**}P = 0.0015$ (scrambled versus siRNA 2), ANOVA. Data are mean ± s.d. AKT molecular mass, 60 kDa. **h**, Invasion quantification of 67NR cancer cell spheroids co-cultured with DRG neurons in the presence of small-molecule inhibitors of PI3K signalling (10 nM, 100 nM or 1 μM). $^{***}P = 0.0005$, $^{****}P < 0.0001$, Kruskal–Wallis test. Data are mean ± s.d. Scale bars, 200 μm (**f**), 100 μm (**a**), 50 μm (**c** and **h**) and 25 μm (**b**).

Pretreatment of 67NR cancer cells with DRG-CM supplemented with RNase inhibited the ability of DRG-CM to confer a metastasis-promoting phenotype (Fig. 3g). In further support of the pro-metastatic effects of this axis, we found that SP and ssRNA40 promoted the invasiveness of spheroids from two additional mouse breast cancer cell lines (4T1 and Py8119 cells) and a human breast cancer cell line (MDA-MB-231) (Extended Data Fig. 8a,b).

Neuronal SP could induce ssRNA release by cancer cells either through a regulated secretory pathway or by cell death. In support of the latter model, we identified a small (<1% of spheroid area) but significant increase in cancer cell apoptosis after co-culture with neurons or after treatment with SP (Fig. 3h). By contrast, the neuropeptide galanin did not promote cancer cell death (Extended Data Fig. 9a). Importantly, addition of a pan-caspase inhibitor (z-VAD-FMK) blocked the pro-invasive effects of both DRG co-culture and SP treatment (Fig. 3i). While co-culture with DRG neurons and SP treatment increased the amount of RNA released into the conditioned medium, addition of z-VAD-FMK prevented RNA release (Fig. 3j). Collectively, these data support a model in which DRG neurons release SP, which induces apoptosis in a subset of cancer cells and subsequent ssRNA release.

Using immunofluorescence and flow cytometry analyses, we found that a small subpopulation of cancer cells expressed high levels of the SP receptor TACR1 (Extended Data Fig. 9b,c). We hypothesized that these TACR1^{high} cells may be most susceptible to cell death after SP treatment. Consistent with this, we found an approximately 40% reduction in the number of TACR1^{high} cancer cells after co-culture with DRG neurons or SP treatment (Extended Data Fig. 9b,c), suggesting that heterogeneous expression of tumoural TACR1 underlies heterogeneous cell death after SP exposure. In further support of this, depletion of tumoural TACR1 suppressed the ability of SP to induce cell death (Extended Data Fig. 9d,e) and invasion (Extended Data Fig. 9f). Taken together, these data demonstrate that neuronal SP causes cell death in a subpopulation of TACR1^{high} cancer cells, causing release of ssRNAs that drive metastasis.

Sensory nerves signal through tumoural TLR7

We next sought to define the mechanism by which extracellular ssRNAs promote breast cancer metastasis. In mice, ssRNAs are detected by Toll-like receptor 7 (TLR7), which mediates innate immune RNA sensing and effector responses[30]. To determine whether tumoural TLR7 mediates the downstream prometastatic effects of ssRNAs, we depleted *Tlr7* in 67NR cancer cells before co-culture with primary DRG neurons (Extended Data Fig. 9g). TLR7-depleted breast cancer spheroids did not exhibit enhanced invasiveness or proliferation after co-culture with DRG neurons (Fig. 4a,b). In contrast, tumour

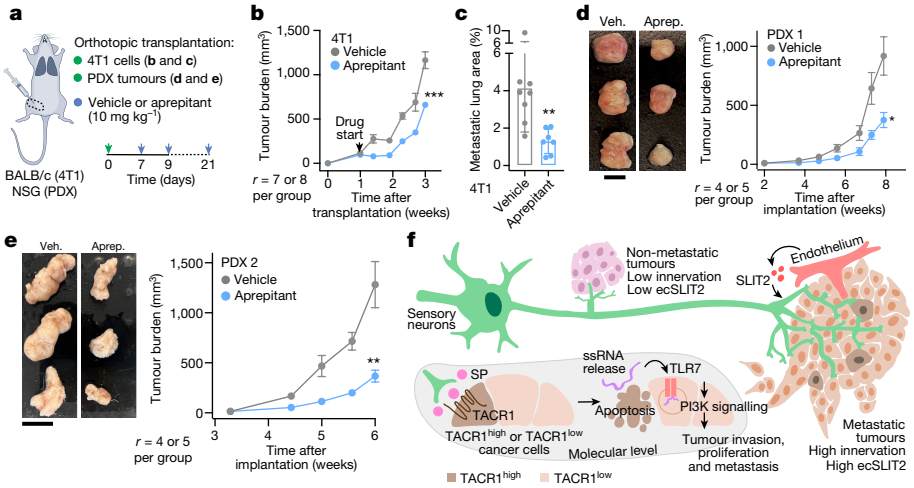

Fig. 5 | The antiemetic aprepitant targets this neuro–cancer axis to inhibit metastasis. a–**e**, The clinically used anti-nausea medication aprepitant was evaluated for its potential in inhibiting breast cancer progression and metastasis. **a**, Schematic of TACR1 antagonism in vivo. 4T1: orthotopic tumour, aprepitant delivered intratumourally. PDXs: subcutaneous tumour, aprepitant delivered intraperitoneally. **b**, 4T1 tumour growth. ***$P = 0.0003$, Mann–Whitney U-test. Data are mean ± s.e.m. **c**, The 4T1 metastatic area was quantified on the basis of H&E staining. **$P = 0.0086$, Student's t-test. Data are mean ± s.d. $r = 7$–8 mice per group. **d**,**e**, Tumour growth for two independent PDX models. *$P = 0.0116$, **$P = 0.0037$, Student's t-test. Data are mean ± s.e.m. **f**, The model. Breast tumours are frequently innervated by sensory nerves. Metastatic breast tumours have more sensory innervation than isogeneic tumours with lower metastatic potential. SLIT2 (reddish pink circles) from the vasculature regulates tumour innervation. In the tumour stroma, neuronal SP (pink circles) causes cell death in a subset of TACR1^{high} cancer cells (dark brown), causing ssRNA release that acts in a paracrine manner on tumoural TLR7 receptors (double reddish pink vertical bars) of neighbouring cancer cells to drive breast cancer metastasis. Scale bars, 1 cm (**d** and **e**).

spheroids lacking the dsRNA sensor TLR3 co-cultured with DRGs retained their invasiveness (Extended Data Fig. 9h,i). Additionally, SP was unable to promote invasion of *Tlr7*-depleted 67NR spheroids (Fig. 4c), suggesting signalling through a shared axis. Treatment of 67NR spheroids with synthetic TLR7 agonists such a R837 (imiquimod, TLR7-specific agonist) or R848 (resiquimod, TLR7/8 dual-agonist) also significantly increased spheroid invasion (Extended Data Fig. 9j). Moreover, lentiviral shRNA-mediated depletion of *Tlr7* in 4T1 cancer cells reduced spheroid invasion in vitro (Extended Data Fig. 9k,l) and tumour growth and metastasis in vivo (Fig. 4d–f). The antimetastatic effects of *Tlr7* depletion were immune independent as (1) we did not observe changes in the abundance of tumour-infiltrating CD45$^+$, CD3$^+$ or NK1.1$^+$ immune cells after TLR7 loss (Extended Data Fig. 9m), and (2) loss of TLR7 significantly reduced tumour growth and metastasis in immune-compromised NSG mice (Extended Data Fig. 9n–p). Importantly, RNase A treatment of TLR7-depleted 4T1 tumours did not further reduce tumour growth (Extended Data Fig. 9q–s), consistent with a common pathway comprising ssRNA and TLR7. Taken together, these data reveal that neuron-dependent release of ssRNA species from cancer cells signals in a paracrine manner through TLR7 to drive invasion, growth and metastasis.

To define the tumoural gene expression response downstream of TLR7 activation, we performed mRNA-sequencing analysis of control and TLR7-depleted 4T1 spheroids (Extended Data Fig. 10a). Gene set enrichment analysis (GSEA) revealed that TLR7 depletion repressed expression of genes implicated in cancer cell invasion, proliferation and metastasis—notably, focal adhesion genes, extracellular matrix receptors and components of the PI3K–AKT signalling pathway (Extended Data Fig. 10a). TLR7 is the predominant sensor for pathogen-derived ssRNAs and canonically activates a MYD88-dependent inflammatory cytokine response in immune cells[31]. Given the absence of an inflammatory gene signature after TLR7 depletion in cancer cells, we hypothesized that TLR7 was signalling through a non-canonical MYD88-independent pathway. Consistent with this, depletion of MYD88 from 67NR cancer cell spheroids did not alter the ability of DRG neurons to promote invasion (Extended Data Fig. 10b,c).

Non-canonical PI3K signalling downstream of TLR activation has been observed in certain cell types (such as macrophages[32]) or certain disease contexts (such as myocardial ischaemia[33]). Given that PI3K–AKT signalling was one of the top downregulated pathways after tumoural TLR7 depletion (Extended Data Fig. 10a), we hypothesized that PI3K may be activated downstream of neuronal activation of tumoural TLR7 receptors. Consistent with this, TLR7 depletion in cancer cells significantly reduced the levels of phosphorylated AKT (pAKT) (Fig. 4g). Importantly, three independent small-molecule inhibitors of PI3K signalling (buparlisib, capivasertib and pictilisib) prevented DRG neuron-induced cancer spheroid invasiveness in a dose-dependent manner (Fig. 4h). All three PI3K inhibitors also prevented SP-induced cancer spheroid invasiveness (Extended Data Fig. 10d). Taken together, these data implicate PI3K signalling as a MYD88-independent mechanism downstream of TLR7 that confers pro-invasive phenotypes onto breast cancer cells.

To further assess the role of this signalling axis in human metastatic disease, we calculated a gene expression signature based on transcripts that were differentially expressed after *Tlr7* depletion and used it to stratify survival of patients with breast cancer. In multivariate analyses conducted across both the TCGA and the METABRIC cohorts, we found that the *Tlr7*^{high} signature correlated with reduced overall survival (METABRIC: hazard ratio = 1.616, $P = 0.024$; TCGA: hazard ratio = 2.730, $P = 0.001$; Extended Data Fig. 10e,f). These findings reveal that TLR7 promotes a prometastatic gene expression program that is associated with reduced survival of patients with breast cancer.

Aprepitant inhibits this neuro–cancer axis

Our results demonstrate a crucial role for neuronal SP and its receptor TACR1 in driving breast cancer metastatic progression. Aprepitant is a small-molecule therapeutic drug that acts as an antagonist of TACR1 and is used clinically to treat nausea[34]. The effect of TACR1 antagonism on cancer cell proliferation and invasion in traditional 2D culture models has yielded conflicting results[35–38]. In our in vitro 3D culture models, aprepitant significantly decreased invasiveness of 4T1, Py8119 and

MDA-MB-231 spheroids in a dose-dependent manner (Extended Data Fig. 11a). Administration of clinically relevant doses of aprepitant to mice significantly inhibited tumour growth and metastatic progression in multiple models, including 4T1 cancer cells (Fig. 5a–c), Py8119 cancer cells (Extended Data Fig. 11b,c) and MMTV-PyMT organoids (Extended Data Fig. 11b,d). Aprepitant also significantly impaired tumour growth in two independent PDX models (Fig. 5d,e). Taken together, our findings identify a neuronal-activity-dependent, metastasis-promoting axis comprising SP, TACR1, ssRNA and TLR7. We also provide a proof of concept for therapeutic targeting of multiple nodes in this axis, including an approved anti-nausea medication.

Progression of cancers from neoplastic lesions is associated with an increase in nerve density[1,39]. Cancer cells are known to express neurotrophic factors that drive neuriteogenesis[1,40,41]. In this study, we demonstrate a role for stromal cells in regulating the extent of tumour innervation. We find that an axon-guidance molecule, SLIT2, expressed by the tumour endothelium drives innervation. Within tumours, nerves have been recognized as critical signalling structures that can elicit tumorigenic effects[4,9,10,39,42,43] or tumour-suppressive effects[42,44,45]. The mammary gland receives abundant sensory fibre input[13,14], yet the mechanism by which sensory innervation could regulate breast cancer progression remained poorly characterized. Conceptually, our study reveals the critical dependency of breast tumours on sensory innervation for tumour growth, invasion and metastatic progression. We found that neuronal SP elicits the release of ssRNAs from a minority of TACR1^{high} apoptotic cancer cells. The released ssRNA acts in a paracrine manner on tumoural TLR7 receptors to promote metastasis (Fig. 5f), therefore linking neuropeptide secretion to RNA release and subsequent innate RNA sensing in the tumour compartment. We observed that neuropeptide-mediated activation of TLR7 in cancer cells drives a non-canonical PI3K-dependent gene expression signature that is associated with worse survival outcomes in patients with breast cancer. This study provides direct molecular evidence that links neuronal activity to extracellular RNA-mediated activation of a key oncogenic signalling pathway in an epithelial tumour.

Neuronal activity within the central and peripheral nervous system regulates various aspects of tissue homeostasis, plasticity and immune cell function[46]. Gliomas, for example, have been found to integrate into neuronal circuits in the brain and depend on neuronal activity for tumour growth[7,8]. Certain head and neck cancers can reprogram innervating sensory nerves into a more adrenergic state to support tumour growth[47]. Our data reveal an instructive role for cancer cells of an epithelial origin in altering neuronal activity. Breast cancer cells, in turn, take advantage of this increased neuronal activity to enhance multiple metastatic phenotypes in an activity-dependent manner.

Neurons are evolutionarily conserved modulators of immunity and their immune-regulatory functions have been shown to be critical in tumorigenesis[11,12,42,48,49]. In contrast to these previously reported indirect effects on the tumour stroma, we observed protumorigenic effects of innervation directly on cancer cells through the activation of tumoural TLR7 signalling. While TLR7 canonically functions as a ssRNA pathogen sensor in innate immunity[31], we identified a non-canonical, immune-independent, tumour-intrinsic and metastasis-associated transcriptional response after neuronally-induced TLR7 activation in these cancer cells. Such an ability of cancer cells to selectively exploit tumorigenic responses downstream of innate immune receptors while repressing immune activating responses has been previously described[15,50]. These findings also raise the possibility that pathogenic RNAs that emerge during viral infections may trigger or accelerate metastatic progression through tumoural TLR7 activation.

This research focused on the cancer-cell-intrinsic mechanisms through which sensory neurons regulate breast cancer metastasis and led to the identification of aprepitant as a disruptor of the functional interactions between sensory nerves and breast cancer cells. Given the safety and tolerability of aprepitant, our findings warrant investigations into the clinical efficacy of this agent after its prolonged use in breast cancer in combination with standard of care regimens as an anti-metastatic therapeutic approach.

Online content

Any methods, additional references, Nature Portfolio reporting summaries, source data, extended data, supplementary information, acknowledgements, peer review information; details of author contributions and competing interests; and statements of data and code availability are available at https://doi.org/10.1038/s41586-024-07767-5.

1. Ayala, G. E. et al. Cancer-related axonogenesis and neurogenesis in prostate cancer. *Clin. Cancer Res.* **14**, 7593–7603 (2008).
2. Huang, D. et al. Nerve fibers in breast cancer tissues indicate aggressive tumor progression. *Medicine* **93**, e172 (2014).
3. Oertel, H. Innervation and tumour growth: a preliminary report. *Can. Med. Assoc. J.* **18**, 135–139 (1928).
4. Renz, B. W. et al. β_2 adrenergic-neurotrophin feedforward loop promotes pancreatic cancer. *Cancer Cell* **34**, 863–867 (2018).
5. Latil, A. et al. Quantification of expression of netrins, slits and their receptors in human prostate tumors. *Int. J. Cancer* **103**, 306–315 (2003).
6. Osswald, M. et al. Brain tumour cells interconnect to a functional and resistant network. *Nature* **528**, 93–98 (2015).
7. Venkatesh, H. S. et al. Neuronal activity promotes glioma growth through neuroligin-3 secretion. *Cell* **161**, 803–816 (2015).
8. Venkatesh, H. S. et al. Electrical and synaptic integration of glioma into neural circuits. *Nature* **573**, 539–545 (2019).
9. Zhao, C. M. et al. Denervation suppresses gastric tumorigenesis. *Sci. Transl. Med.* **6**, 250ra115 (2014).
10. Magnon, C. et al. Autonomic nerve development contributes to prostate cancer progression. *Science* **341**, 1236361 (2013).
11. Balood, M. et al. Nociceptor neurons affect cancer immunosurveillance. *Nature* **611**, 405–412 (2022).
12. Globig, A. M. et al. The β_1-adrenergic receptor links sympathetic nerves to T cell exhaustion. *Nature* **622**, 383–392 (2023).
13. Gerendai, I. et al. Transneuronal labelling of nerve cells in the CNS of female rat from the mammary gland by viral tracing technique. *Neuroscience* **108**, 103–118 (2001).
14. Hebb, C. & Linzell, J. L. Innervation of the mammary gland. A histochemical study in the rabbit. *Histochem. J.* **2**, 491–505 (1970).
15. Tavora, B. et al. Tumoural activation of TLR3–SLIT2 axis in endothelium drives metastasis. *Nature* **586**, 299–304 (2020).
16. Brose, K. et al. Slit proteins bind Robo receptors and have an evolutionarily conserved role in repulsive axon guidance. *Cell* **96**, 795–806 (1999).
17. Nguyen-Ngoc, K. V. et al. ECM microenvironment regulates collective migration and local dissemination in normal and malignant mammary epithelium. *Proc. Natl Acad. Sci. USA* **109**, E2595–E2604 (2012).
18. Aslakson, C. J. & Miller, F. R. Selective events in the metastatic process defined by analysis of the sequential dissemination of subpopulations of a mouse mammary tumor. *Cancer Res.* **52**, 1399–1405 (1992).
19. Bujak, J. K., Kosmala, D., Szopa, I. M., Majchrzak, K. & Bednarczyk, P. Inflammation, cancer and immunity-implication of TRPV1 channel. *Front. Oncol.* **9**, 1087 (2019).
20. Liebig, C., Ayala, G., Wilks, J. A., Berger, D. H. & Albo, D. Perineural invasion in cancer: a review of the literature. *Cancer* **115**, 3379–3391 (2009).
21. Kastin, A. *Handbook of Biologically Active Peptides* (Academic, 2013).
22. Otsuka, M. & Konishi, S. Release of substance P-like immunoreactivity from isolated spinal cord of newborn rat. *Nature* **264**, 83–84 (1976).
23. Eshete, F. & Fields, R. D. Spike frequency decoding and autonomous activation of Ca^{2+}-calmodulin-dependent protein kinase II in dorsal root ganglion neurons. *J. Neurosci.* **21**, 6694–6705 (2001).
24. Nishikawa, S. et al. Two histidine residues are essential for ribonuclease T1 activity as is the case for ribonuclease A. *Biochemistry* **26**, 8620–8624 (1987).
25. Robertson, H. D., Webster, R. E. & Zinder, N. D. Purification and properties of ribonuclease III from *Escherichia coli*. *J. Biol. Chem.* **243**, 82–91 (1968).
26. Bremnes, R. M., Sirera, R. & Camps, C. Circulating tumour-derived DNA and RNA markers in blood: a tool for early detection, diagnostics, and follow-up? *Lung Cancer* **49**, 1–12 (2005).
27. Huang, W. et al. Site-specific RNase A activity was dramatically reduced in serum from multiple types of cancer patients. *PLoS ONE* **9**, e96490 (2014).
28. De Lamirande, G. Action of deoxyribonuclease and ribonuclease on the growth of Ehrlich ascites carcinoma in mice. *Nature* **192**, 52–54 (1961).
29. Ledoux, L. Action of ribonuclease on two solid tumours in vivo. *Nature* **176**, 36–37 (1955).
30. Lund, J. M. et al. Recognition of single-stranded RNA viruses by Toll-like receptor 7. *Proc. Natl Acad. Sci. USA* **101**, 5598–5603 (2004).
31. Kawasaki, T. & Kawai, T. Toll-like receptor signaling pathways. *Front. Immunol.* **5**, 461 (2014).
32. Ojaniemi, M. et al. Phosphatidylinositol 3-kinase is involved in Toll-like receptor 4-mediated cytokine expression in mouse macrophages. *Eur. J. Immunol.* **33**, 597–605 (2003).
33. Ha, T. et al. TLR2 ligands induce cardioprotection against ischaemia/reperfusion injury through a PI3K/Akt-dependent mechanism. *Cardiovasc. Res.* **87**, 694–703 (2010).

34. Hesketh, P. J. et al. The oral neurokinin-1 antagonist aprepitant for the prevention of chemotherapy-induced nausea and vomiting: a multinational, randomized, double-blind, placebo-controlled trial in patients receiving high-dose cisplatin-the Aprepitant Protocol 052 Study Group. *J. Clin. Oncol.* **21**, 4112–4119 (2003).
35. Rosso, M., Robles-Frias, M. J., Covenas, R., Salinas-Martin, M. V. & Munoz, M. The NK-1 receptor is expressed in human primary gastric and colon adenocarcinomas and is involved in the antitumor action of L-733,060 and the mitogenic action of substance P on human gastrointestinal cancer cell lines. *Tumour Biol.* **29**, 245–254 (2008).
36. Munoz, M. & Rosso, M. The NK-1 receptor antagonist aprepitant as a broad spectrum antitumor drug. *Invest. N. Drugs* **28**, 187–193 (2010).
37. Nagakawa, O. et al. Effect of prostatic neuropeptides on invasion and migration of PC-3 prostate cancer cells. *Cancer Lett.* **133**, 27–33 (1998).
38. Nizam, E. & Erin, N. Differential consequences of neurokinin receptor 1 and 2 antagonists in metastatic breast carcinoma cells; effects independent of substance P. *Biomed. Pharmacother.* **108**, 263–270 (2018).
39. Le, T. T. et al. Sensory nerves enhance triple-negative breast cancer invasion and metastasis via the axon guidance molecule PlexinB3. *NPJ Breast Cancer* **8**, 116 (2022).
40. Austin, M., Elliott, L., Nicolaou, N., Grabowska, A. & Hulse, R. P. Breast cancer induced nociceptor aberrant growth and collateral sensory axonal branching. *Oncotarget* **8**, 76606–76621 (2017).
41. Jurcak, N. R. et al. Axon guidance molecules promote perineural invasion and metastasis of orthotopic pancreatic tumors in mice. *Gastroenterology* **157**, 838–850 (2019).
42. Kamiya, A. et al. Genetic manipulation of autonomic nerve fiber innervation and activity and its effect on breast cancer progression. *Nat. Neurosci.* **22**, 1289–1305 (2019).
43. Zahalka, A. H. et al. Adrenergic nerves activate an angio-metabolic switch in prostate cancer. *Science* **358**, 321–326 (2017).
44. Partecke, L. I. et al. Subdiaphragmatic vagotomy promotes tumor growth and reduces survival via TNFα in a murine pancreatic cancer model. *Oncotarget* **8**, 22501–22512 (2017).
45. Renz, B. W. et al. Cholinergic signaling via muscarinic receptors directly and indirectly suppresses pancreatic tumorigenesis and cancer stemness. *Cancer Discov.* **8**, 1458–1473 (2018).
46. Boilly, B., Faulkner, S., Jobling, P. & Hondermarck, H. Nerve dependence: from regeneration to cancer. *Cancer Cell* **31**, 342–354 (2017).
47. Amit, M. et al. Loss of p53 drives neuron reprogramming in head and neck cancer. *Nature* **578**, 449–454 (2020).
48. Kalinichenko, V. V., Mokyr, M. B., Graf, L. H. Jr, Cohen, R. L. & Chambers, D. A. Norepinephrine-mediated inhibition of antitumor cytotoxic T lymphocyte generation involves a β-adrenergic receptor mechanism and decreased TNF-α gene expression. *J. Immunol.* **163**, 2492–2499 (1999).
49. Mohammadpour, H. et al. β2 adrenergic receptor-mediated signaling regulates the immunosuppressive potential of myeloid-derived suppressor cells. *J. Clin. Invest.* **129**, 5537–5552 (2019).
50. Benci, J. L. et al. Opposing functions of interferon coordinate adaptive and innate immune responses to cancer immune checkpoint blockade. *Cell* **178**, 933–948 (2019).

Methods

Animal studies

All animal experiments were conducted in accordance with the Institutional Animal Care and Use Committee (IACUC) at The Rockefeller University. All animals were housed at ambient temperature in a 12 h–12 h light–dark cycle with unrestricted access to food and water. Female mice were age matched; litter mates were used when possible and animals were randomized to each experimental cohort. No statistical methods were used to predetermine sample sizes. All tumour growth studies were performed in accordance with IACUC guidelines and mice were euthanized when the tumour volume exceeded 1,500 mm^3. Tumour measurements and metastasis quantification were performed in a blinded manner. Wild-type BALB/cJ, C57BL/6J, FVB, NSG, Tac1-null[51] (JAX, 004103) and Nav1.8-Cre (JAX, 036564) mice were obtained from Jackson Laboratories. The endothelial-specific inducible Cre line *Cdh5(PAC)-creERT2* was obtained from R. Adams[52]. *Cdh5(PAC)-creERT2;Slit2$^{fl/fl}$* mice were crossed for at least six generations with pure wild-type BALB/cJ mice. To activate Cre, mice were injected intraperitoneally with 150 µl of tamoxifen diluted in corn oil (10 mg ml^{-1}) for 2 consecutive days. Concomitantly, mouse chow was replaced with tamoxifen-supplemented food (250 mg per kg) (Envigo, TD.130856). MMTV-PyMT[53] mice were a gift from K. J. Cheung. Fixed C3(1)-Tag[54] tumours were donated by A. J. Ewald. Live PDXs used in this study were obtained from Jackson Laboratories (TNM00096 and TNM00098) and were maintained subcutaneously in NSG mice. PDX tumours were implanted by Jackson Laboratories before shipment to Rockefeller University; tumours were <100 mm^3 when aprepitant[55] treatments were initiated. PDX sections from patients with breast cancer were obtained from A.L. Welm.

Human samples

All research involving human samples at Rockefeller University is supervised by the Institutional Review Board (IRB). This study was found to be IRB-exempt. All human tumour samples used in the study were received from the Cooperative Human Tissue Network (CHTN). The samples used in Fig. 1a and Extended Data Fig. 2j–m were received in basal medium the day after surgery. The samples used for western blotting ($n = 11$) were snap-frozen after arrival and stored at −80 °C until use. The samples used in Figs. 1b and 2f ($n = 19$) were received as formalin-fixed paraffin-embedded (FFPE) blocks or sections and were processed for immunofluorescence analysis. Deidentified pathology information for each of these samples was used to determine the lymph node status of the patient.

Primary DRG culture

DRG neurons were isolated from 5–8-week-old female syngeneic mice (BALB/cJ, FVB or C57BL/6J). Each mouse was perfused with 20 ml of cold HBSS (Sigma-Aldrich, 55021C). Ganglia were collected into cold HBSS and pelleted by centrifuging at 100*g* for 2 min. Ganglia were then digested in papain (Worthington, LS003126) and collagenase (Worthington, LS004176) at 37 °C. The digested neurons were triturated with fire-polished Pasteur pipettes. DRG neurons were further purified using a Percoll (GE Healthcare, 17-0891-01) gradient (12.5% and 28%). Pelleted neurons were resuspended in neuronal growth medium (NGM; DMEM-F12 with HEPES (Thermo Fisher Scientific, 11-330-032)), penicillin–streptomycin (Thermo Fisher Scientific, 15140-122), bovine serum albumin (BSA; Sigma-Aldrich, A9576), and fetal bovine serum (FBS; Sigma-Aldrich, F4135) at a concentration of 50–100 neurons per µl. For all co-culture experiments, a DRG:cancer cell ratio of 1:200 was used unless specified otherwise.

Isolation of primary tumour organoids

Human or mouse mammary tumours were processed into organoids as previously described[56]. Samples were mechanically disrupted with a scalpel, and enzymatically (collagenase-based) digested. The digested tissue was centrifuged for 10 min at 1,500 rpm. The pelleted tissue was then treated with DNase (Sigma-Aldrich, D4263). Differential centrifugations (quick spins at 400*g* for 3–7 s) were used to separate out single/stromal cells from epithelial organoids.

Tissue culture and spheroid generation

4T1, EO771, HEK293T, Py8119 and MDA-MB-231 cells were obtained from American Tissue Type Collection (ATCC). 4T07 and 67NR cells were a gift from W. P. Schiemann. EO771 cells were maintained in RPMI with 10% FBS and 10 mM HEPES (Thermo Fisher Scientific, 15-630-080). 67NR, 4T1 and MDA-MB-231 cancer cells were maintained in DMEM (Gibco, 11995065) with 10% FBS. Py8119 cells were cultured in Ham's F-12K (Kaighn's) medium (Thermo Fisher Scientific, 21127022) with 10% FBS. Contamination with mycoplasma was ruled out on a quarterly basis using PCR-based protocols[57].

Spheroids were formed using the hanging-drop method[58]. In total, 50, 3,000 and 1,500 cells from 4T1, 67NR and Py8119, respectively, were resuspended in 25 µl of medium and plated into the lid of a tissue-culture-treated dish. For MDA-MB-231 spheroids, 5,000 cells were resuspended in 25 µl of medium containing 5% Matrigel (Corning, 354320). Droplets were placed sufficiently apart to not merge when lid was inverted and placed back on the PBS-filled reservoir. Spheroids were collected after an overnight incubation.

3D cultures

For invasion assays, organoids/spheroids were embedded in neutralized, cold-polymerized, fibrillar rat-tail collagen I (Corning, 354236). Invasion assays in the presence of DRG neurons consisted of 100 neurons per well in a 24-well plate. The end point for 3D invasion assays involving cancer cell lines was around 48–72 h, while that for cultures involving MMTV-PyMT or primary human tumour organoids was about 5 days. For colony-formation assays using the MMTV-PyMT mouse model, organoids were briefly dissociated into small cell clusters and embedded in Matrigel (Corning, 354320; 5,000 clusters per well in a 24-well plate). For cell lines, colony-formation assays were performed using 67NR cancer cells (10,000 cells per well in a 24-well plate) and DRG neurons (100 neurons per well in a 24-well plate). The base medium for all organoid cultures (and co-cultures) included DMEM (Gibco, 11995065), L-glutamine (Thermo Fisher Scientific, 35050061), 1% penicillin–streptomycin (Gibco, 15070063), 0.2% BSA (Sigma-Aldrich, A9576), FBS (Sigma-Aldrich, F4135), and N2 and B27 supplements (Thermo Fisher Scientific, 17502048 and 17504001, respectively), and is referred to as neuronal growth medium (NGM). Human organoids were additionally supplemented with hEGF (Sigma-Aldrich, E9644), whereas mouse organoid cultures were supplemented with FGF2 (Sigma-Aldrich, F0291). Conditioned medium was collected at 24 and 48 h after the setup of the original 3D culture in collagen I. Conditioned medium was collected and replaced with fresh NGM. For conditioned medium experiments, RNase A (Thermo Fisher Scientific, EN0531) was used at a concentration of 25 µg ml^{-1}, RNase T1 (Thermo Fisher Scientific, EN0541) was used at a concentration of 2,000 U ml^{-1}, RNase III (Thermo Fisher Scientific, AM2290) was used at a concentration of 2.5 U ml^{-1}, DNase I was used at a concentration of 2 U ml^{-1} and heat inactivation was performed at 100 °C for 20 min. For ssRNA/dsRNA mimetic experiments, ssRNA40 (ref. 59) (InvivoGen, tlrl-lrna40) and poly(I:C)[60] (InvivoGen, tlrl-pic) were used at concentrations of 0.5, 1 and 5 µg ml^{-1}. ssRNA40 is complexed with the cationic lipid LyoVec to facilitate its uptake. Furthermore, the two imidazoquinoline amines, imiquimod[61] (R837, TLR7 agonist, Selleckchem, S1211) and resiquimod[62] (R848, TLR 7/8 agonist, Selleckchem, S8133) were used at concentrations of 1 and 10 µg ml^{-1} for TLR7 stimulation. For apoptosis blockage the pan-caspase inhibitor z-VAD-FMK (Selleckchem, S7023) was used at a concentration of 100 µM. PI3K–AKT signalling was inhibited using buparlisib[63],

capivasertib[64] or pictilisib[65] at 0.01–1 μM concentrations as noted in the figures.

Matrigel Transwell invasion assay

67NR cancer cells were serum-starved in 0.2% FBS DMEM overnight. The next day, Matrigel Invasion Chambers (Corning, 354483) were rehydrated with 0.2% FBS DMEM for 2 h at 37 °C. Meanwhile, 750 μl of NGM was added to wells of a 24-well plate and seeded with either 1,000 DRG neurons or 100 nM SP. The starved cancer cells were resuspended at 2.5×10^4 cells per ml in 0.1% BSA DMEM. Matrigel invasion chambers were emptied after rehydration, transferred to wells containing NGM, and 500 μl of cells (1.25×10^4) were added to the chamber. Cells were allowed to invade for 24 h at 37 °C. The medium was then removed from the Matrigel inserts and the inserts were washed with PBS to remove cancer cells that did not invade. Inserts were fixed in 4% paraformaldehyde for 30 min followed by a PBS wash. The inserts were stained with 0.1% crystal violet, washed three times in PBS and invaded cells were counted in five fields of view using the ×10 objective on the inverted Primo Vert (Zeiss) microscope.

Lentiviral production and transduction

A third-generation lentivirus system was used to produce virus from HEK293T cells grown in 10 cm plates. HEK293T cells were plated at 70% confluency the night before transfection and cultured in DMEM (Gibco, 11995065) with 10% FBS (Sigma-Aldrich, F4135). Cells were transfected with 2.5 μg of Gag-Pol, 5 μg of VSV-G, 2.5 μg of RSV-Rev (Cell Biolabs, VPK-205) and 7.5 μg of pLKO.puro1 vector (Sigma-Aldrich) cloned to contain the appropriate shRNA, using 60 μl of Lipofectamine 2000 (Thermo Fisher Scientific, 11668019). After an overnight incubation, the medium was replaced with fresh medium. Virus-containing medium was collected at 48 h and 72 h after transfection. The supernatant was filtered through a 0.45 μm filter (Pall, 4614), mixed 1:1 with fresh medium and substituted with 8 μg ml^{-1} polybrene (Sigma-Aldrich, TR-1003-G) to transduce preplated 4T1 cells at 50% confluency. Selection with 2.5 μg of puromycin (Thermo Fisher Scientific, A1113803) was conducted 36 h after transduction. Knockdown was validated using quantitative PCR (qPCR) and western blotting.

The following shRNAs were used: *Tlr7* shRNA 1 (mouse): F, 5′-CCGGTCTATGGAGAGCCGGTGATAACTCGAGTTATCACCGGCTCTCCATAGATTTTTG-3′; R, 5′AATTCAAAAATCTATGGAGAGCCGGTGATAACTCGAGTTATCACCGGCTCTCCATAGA-3′; *Tlr7* shRNA 2 (mouse): F, 5′-CCGGACCACTTTGCCACCTAATTTACTCGAGTAAATTAGGTGGCAAAGTGGTTTTTTG-3′; R, 5′AATTCAAAAAACCACTTTGCCACCTAATTTACTCGAGTAAATTAGGTGGCAAAGTGGT-3′; *Tacr1* shRNA 1 (mouse): F, 5′-CGGGAGGACAGTGACCAATTATTTCTCGAGAAATAATTGGTCACTGTCCTCTTTTTG-3′; R, 5′-AATTCAAAAAGAGGACAGTGACCAATTATTTCTCGAGAAATAATTGGTCACTGTCCTC-3′; *Tacr1* shRNA 2 (mouse): F, 5′-CCGGTGGAGAAGGCAAGCGTTATATCTCGAGATATAACGCTTGCCTTCTCCATTTTTG-3′; R, 5′-AATTCAAAAATGGAGAAGGCAAGCGTTATATCTCGAGATATAACGCTTGCCTTCTCCA-3′.

siRNA transfection

Transient knockdown of *Tlr7* was performed using at least two independent siRNAs against these genes in 67NR cells (the sequences are listed below). The siRNA and Lipofectamine RNAiMAX transfection reagent (Thermo Fisher Scientific, 13778150) were diluted in Opti-MEM (Thermo Fisher Scientific, 31985070) and added to 67NR cells at around 60% confluency. After an overnight incubation, the culture medium was replaced with fresh medium. Successful knockdown was validated using qPCR and western blotting.

The following siRNAs were used: *Tlr7* (mouse): 5′-GCAGAAGGAAUUACUCACAUGCUAA-3′; 5′-CCUUUCAGUGAAUAAGAUAUCUCCT-3′; *Myd88* (mouse): 5′-UGGUUGUUUCUGACGAUUAUCUACA-3′; 5′-UGUUAGACCGUGAGGAUAUACUGAA-3′; 5′-AGGUUUGCAUCUUCUUAUUCCUUTC-3′.

Protein Isolation

Cell lines were washed with and scraped into ice-cold PBS (without any Ca^{2+} or Mg^{2+}), centrifuged for 5 min at 300*g* (4 °C). The cell pellet was resuspended in an appropriate volume of RIPA-based lysis buffer, vortexed and left on ice for 5 to 10 min. For primary tumours, ~10 mg of tumour tissue was homogenized in ~100 μl ice-cold RIPA lysis buffer using an electric homogenizer (Bel-Art Homogenizer System, Thermo Fisher Scientific, 03-421-215; Bel-Art Pestles and Tubes, Thermo Fisher Scientific, 03-421-221). The samples were centrifuged at 10,000*g* (4 °C) for 10 min and the supernatants were transferred to new, prechilled Eppendorf tubes. A BCA assay kit (Thermo Fisher Scientific, PI23225) was used to quantify the amount of protein in each sample. The samples were stored at −80 °C.

Western blotting

Whole-cell protein lysates were thawed on ice for 30 min before use. The samples were diluted with 4× protein loading buffer (Li-Cor, 928-40004) and 10× sample reducing agent (Thermo Fisher Scientific, NP0009). Equal amounts of protein were loaded in 4–12% Bis-tris Mini Protein Gels (Thermo Fisher Scientific, NP0336PK2). SDS–PAGE was performed in MES-SDS running buffer (20×, Thermo Fisher Scientific, NP0002) at 140 V for around 1 h or until the dye front had run off the gel. The gels were transferred at 100 V for 1.5 h at 4 °C in transfer buffer (Thermo Fisher Scientific, NP0006) onto PVDF membranes (Thermo Fisher Scientific, 88520). The membranes were blocked in 5% non-fat dry milk (Bio-Rad, 1706404) in TBS-T (TBS (Cell Signalling Technology, 12498S) + 0.1% Tween-20 (Millipore, P2287)) for 1 h at room temperature. Primary antibodies were diluted in 3% BSA/TBS-T (Millipore, A2153) and incubated overnight at 4 °C. The membranes were washed three times with 0.1% TBS-T and incubated for 1 h at room temperature with corresponding HRP-linked secondary antibodies, added at a dilution of 1:10,000. The membranes were then washed three times with 0.1% TBS-T and activated by an ECL blotting solution (Thermo Fisher Scientific, 32106). X-ray films (Imaging Solutions Company, 110102) were exposed to the membrane from 10 s up to 2 min and developed afterwards. ImageJ was used to quantify the band intensity. The following primary antibodies were used: mouse βIII-tubulin (1:1,000; BioLegend, MMS-435P, TUJ1), rabbit GAPDH (1:1,000; Cell Signalling, 2118, 14C10), mouse HSP-60 (1:1,000; Santa Cruz Biotechnology, sc-13115) and rabbit TACR1 (1:1,000; Thermo Fisher Scientific, PA1-32229). Uncropped western blots are provided in Supplementary Fig. 1.

Immunofluorescence

Tumours, lungs and mammary glands collected from mice were fixed in 4% paraformaldehyde (Thermo Fisher Scientific, AA433689M) overnight at 4 °C and then transferred into 25% sucrose (Sigma-Aldrich, S0389), 0.1% sodium azide (Thermo Fisher Scientific, 71448-16) in PBS for 24 h at 4 °C. Tissues were embedded in Tissue-Tek O.C.T. Compound (VWR, 4583) and frozen at −80 °C. Sections (thickness, 20–50 μm) were cut using a cryostat set to −20 °C cutting temperature for lungs and tumours and −27 °C for mammary glands. The sections were collected onto Superfrost Plus microscope slides (Thermo Fisher Scientific, 12-550-15). Before immunofluorescence staining, O.C.T. was removed by incubating the slides in PBS for 1 h.

FFPE tissue sections were dewaxed and rehydrated using xylene and descending concentrations of ethanol. Antigen retrieval was performed by boiling the samples in citrate buffer (Sigma-Aldrich, C9999) for 30 min. The sections were then permeabilized using 0.5% Triton X-100 (Millipore, T9284). The slides were blocked in 10% FBS (Sigma-Aldrich, F4135), 1% BSA (Millipore, A2153) and 0.1% Tween-20 (Millipore, P2287) in PBS for up to 2 h at room temperature. Incubation with primary and secondary antibodies (diluted in 1% FBS, 1% BSA, 0.1% Tween-20) was performed overnight at 4 °C or for 2–3 h at room temperature. The slides were mounted with Prolong Gold (Thermo Fisher

Scientific, P36930). Primary antibodies used in the study include rabbit anti-CGRP (1:250, Cell Signalling, monoclonal antibody, 14959), mouse anti-βIII-tubulin (1:200, BioLegend, MMS-435P, TUJ1), rabbit anti-Ki-67 (1:250, Abcam, ab15580), rabbit anti-SP (1:200, Sigma-Aldrich, AB1566), mouse anti-neurofilament-L (1:400, NFL, Cell Signalling, 2837), mouse anti-dsRNA (1:200, Axxora, JBS-RNT-SCI-10010200) and phalloidin (1:200, Thermo Fisher Scientific, A12379). Nuclei were counterstained using Hoechst (1:500, Thermo Fisher Scientific, H3579). All secondary antibodies were AlexaFluor conjugates (1:200, Thermo Fisher Scientific, A21206, A21202, A31573, A31572, A31571, A31570 or A21208).

qPCR analysis

RNA was extracted from cells using the RNA purification kit (Norgen Biotek, 37500) according to the manufacturer's protocol. Reverse transcription PCR (RT–PCR) was performed on 2–5 μg of RNA using the SuperScript III First-Strand Synthesis System (Thermo Fisher Scientific, 18080051). RT–qPCR was conducted in a 384-well PCR microplate (Thermo Fisher scientific, AB-1384) on the Applied Biosystem StepOne Real-Time PCR System using the Fast SYBR Green master mix (Thermo Fisher Scientific, 43-856-18). ΔC_t values were used to calculate the relative levels of the mRNA of interest, which were normalized to the mRNA levels of *GAPDH*. Primers used in the studies include:

Gapdh (mouse): forward, 5′-AGGTCGGTGTGAACGGATTTG-3′; reverse, 5′-TGTAGACCATGTAGTTGAGGTCA-3′; *Tlr7* (mouse): forward, 5′-CACCACCAATCTTACCCTTACC-3′; reverse, 5′-CAGATGGTTCAGCCTACGGAA-3′; *Tacr1* (mouse): forward, 5′-CTCCACCAACACTTCTGAGTC-3′; reverse, 5′-TCACCACTGTATTGAATGCAGC-3′; *Tlr3* (mouse): forward, 5′-GTGAGATACAACGTAGCTGACTG-3′; reverse, 5′-TCCTGCATCCAAGATAGCAAGT-3′.

Flow cytometry analysis

All steps were performed on ice and under protection from light. Fresh flow buffer containing 25 mM HEPES (Thermo Fisher Scientific, 11-330-032), 1% BSA (Sigma-Aldrich, A9576), 1% FBS (Sigma-Aldrich, F4135) and 1% penicillin–streptomycin (Thermo Fisher Scientific, 15140-122) in PBS was prepared. 67NR cancer cells were detached from culture dishes, strained through a 70 μm filter, pelleted, washed with ice-cold PBS and incubated in 50 μl of staining buffer (anti-TACR1, 1:200 in flow buffer, alamone labs, ATR-001) for 20 min. Cells were washed three times with 1 ml of flow buffer. The last step was repeated for secondary antibody as well (1:200, Thermo Fisher Scientific, A31572). DAPI (Thomas Scientific, C756W66) was used as a live/dead stain. Flow cytometry data were obtained using the Attune NxT cytometer and data were analysed using FlowJo. The gating strategy is shown in Supplementary Fig. 2.

Mammary fat pad injections

Cancer cells (67NR, 4T1, EO771 or Py8119) were resuspended in a 1:1 mix of PBS:Matrigel (Corning, 354320) at a concentration of 10^6 cells per ml. For DRG co-transplantations, 50 (low), 250 (medium) or 1,000 (high) DRGs were injected per animal (added to the cancer cell suspension just before injections into the animal). Orthotopic transplantations were conducted in 5–7-week-old syngeneic female mice as previously described[66]. Mice were anaesthetized, immobilized and the surgical site was shaved and sterilized using povidone iodine (Abcam, ab143439). A midline incision was made to expose the abdominal mammary gland. 50 μl of the cell suspension was injected into the mammary gland. The surgical wound was closed using 9 mm autoclips (Thermo Fisher Scientific, NC9938480). Tumour measurements were taken using digital callipers twice a week and the tumour volume was calculated according to $r \times h^2/2$. Tumours and lungs were typically collected 3 to 4 weeks after transplantation when the tumour volume reached around 1,500 mm^3, in accordance with our IACUC protocols. Macrometastases (>100 cells) within the lungs were quantified using H&E staining of 5-μm-thick tumour sections. Micrometastases were counted manually in lung sections and typically consist of <50 cells. For circulating tumour cell enumeration, cardiac puncture was used to obtain 750 μl–1 ml of blood from animals with late-stage tumours. After lysis of red blood cells, the remainder of the sample was smeared onto a glass microscope slide and examined under a confocal microscope for $mCherry^+$ expression. Cells with intact nuclei and mCherry expression were identified as circulating tumour cells.

Tail-vein injections

$mCherry^+$ 67NR cancer cells were resuspended in PBS at a concentration of 750,000 cells per ml and stored on ice. Tail-vein injections were performed in 6–9-week-old syngeneic female mice. Mice were placed in a heating chamber set to 37 °C for 10 min and immobilized in a restraining device. Then, 200 μl of the cell suspension was injected through the tail vein. The lungs from these mice were collected around 1 week later and the number of $mCherry^+$ macrometastases were quantified under the dissection microscope.

Intracardiac injections

100,000 $mCherry^+$ 67NR cancer were injected into the left ventricle in 100 μl of PBS using a 26 gauge needle while mice were under 2.5% isoflurane anaesthesia. Then, 2 weeks later, the brain, liver, lungs, femur and ovaries were collected and the number of $mCherry^+$ macrometastases was examined under a dissection microscope.

Intraductal injections

Intraductal injections of cancer cells or reagents/drugs were performed to restrict delivery within the ductal epithelium. Injections were performed under a dissection microscope as previously described[67]. Using a pair of microdissecting tweezers, the dead skin around the nipple was removed. A 33 gauge microsyringe (needle, CAL7637-01; syringe, 89221-012) was used to inject no more than 20 μl into the ductal epithelium. 4T1 cancer cells were resuspended at a concentration of 10^6 cells per ml in PBS. Capsaicin[68] was dissolved in 10% ethanol, 10% Tween-80 and 80% saline and injected into mice (20 μl per mouse) at a concentration of 75 mg per kg. Anti-SP (BioGeneX AR069GP) or IgG control (BioXCell BE0095) antibodies were injected into 4T1 tumour-bearing NOD-SCID gamma mice at a concentration of 20 μg per mouse. RNase A (two sources: Thermo Fisher Scientific, EN0531 and 12091021) was used at a concentration of 5 mg ml^{-1}.

Genotyping of transgenic mouse lines

Tail snips collected from 2.5-week-old mice were lysed in DirectPCR Lysis Reagent (Viagen Biotech, 102-T) and proteinase K (Millipore Sigma, 3115828001) to extract DNA. PCR reactions using the primers listed below were used to detect the presence of a transgene:

MMTV-PyMT: F, 5′-GGAAGCAAGTACTTCACAAGGG-3′; R, 5′-GGAAAGTCACTAGGAGCAGGG-3′; internal positive control, F: 5′-CAAATGTTGCTTGTCTGGTG-3′; internal positive control, R: 5′-GTCAGTCGAGTGCACAGTTT-3′. The positive control runs at 200 bp while the transgene runs at 556 bp.

Tac1-KO: F, 5′-AGAATTTAAAGCTCTTTTGCC-3′; R, 5′-GCTCATCAGTATGTGACATAGAAA-3′. The mutant allele runs at 175 bp while the wild type runs at 190 bp.

Nav1.8-Cre: F, 5′-GGTTCGCAAGAACCTGATGG-3′; R, 5′-GCCTTCTCTACACCTGCGG-3′. This is a generic Cre primer. The transgene runs at 570 bp.

Optical tissue clearing

Clearing of mouse mammary tumours was performed using a previously described AdipoCLEAR protocol[69]. Tumours were fixed in 4% paraformaldehyde (Thermo Fisher Scientific, AA433689M) and washed in increasing concentrations of methanol (20–100%) in B1N buffer (water, 0.1% Triton X-100 (Sigma-Aldrich, T9284), 0.3 M glycine (Sigma-Aldrich, G5417)). Delipidation was performed using 100% dicholoromethane (Sigma-Aldrich, 270997). The samples were washed in decreasing

concentrations of methanol (100–20%) in B1N buffer. Tumours were incubated with primary antibodies (anti-CGRP, 1:200, Cell Signalling, monoclonal antibody, 14959) for 4 days with continuous shaking, then washed overnight and incubated with secondary antibodies (AlexaFluor conjugates) for another 4 days. After immunolabelling, the samples were dehydrated in an increasing series of methanol/water (25–100%). The samples were washed in dicholoromethane overnight and cleared in dibenzyl ether (Sigma-Aldrich, 33630).

Retrograde tracing

GFP-tagged cholera toxin-β[70] was used for retrograde tracing experiments at a concentration of 0.1% in a total injection volume of 20 µl. For the normal mammary gland, CTB was injected intraductally. For tracing experiments in 67NR and 4T1 tumours, CTB was injected intratumourally 2–3 weeks after transplantation. DRGs were isolated from these animals 1 week after CTB injections, fixed in 4% PFA and mounted onto a coverslip.

Imaging and image analysis

Optically cleared tissues were imaged on a light-sheet microscope (LaVision BioTec) with a ×4/0.3 LVMI-Fluar objective with 5.6–6 mm WD. Images were imported into Imaris and rendered in 3D. Confocal microscopy was performed using either the LSM 780 laser-scanning confocal microscope (Zeiss) or A1R confocal microscope (Nikon). Phase-contrast/bright-field images were acquired using the CellDiscoverer7 (Zeiss) microscope. For experiments in which immunofluorescence was used to infer relative protein expression levels, all of the images were collected and processed using identical parameters. All image analysis was performed using ImageJ2, unless stated otherwise below.

(1) The extent of innervation in tissue sections was estimated by manually counting the number of nerve bundles in size-matched tumours, positively identified by βIII-tubulin/neurofilament-L for total innervation analysis, or CGRP for sensory-specific innervation. Two sections per tumour were averaged as a single datapoint in the graphs. Any innervation in the surrounding normal-adjacent tissue was not included in the analysis.

(2) For cleared 3D samples, Imaris (v.10) was used for rendering the maximum-intensity projection image. Autofluorescence (images collected at the 488 nm wavelength) was used to define the tumour boundary.

(3) Proliferation in cancer cell spheroids was assessed as percentage of Ki-67$^+$ nuclei with respect to total number of cells per organoid/spheroid identified by DAPI.

(4) Invasiveness was reported as an inverse of the circularity of the manually traced organoid/spheroid boundary. Circularity is defined as the ratio of the square of the perimeter to 4π times the area. While a circle has a circularity of one, invasive spheroids/organoids have lower circularity scores. Circularity scores are the standard measurement for invasion in 3D cultures as they account for both the number and the length of invasion strands.

(5) The metastatic area was measured by manually tracing the area of metastases as seen by H&E staining of the lung. The total lung area was measured using auto-threshold. The percentage of metastatic area, which accounts for number and size of metastases, was reported. The percentage metastatic area averaged across 3–4 lung sections per mouse was plotted as a single datapoint in the graphs.

(6) For in vivo invasion quantification, we imaged around 20 ROIs within 67NR or 67NR + DRG tumours across three independent tumours per condition. We classified it as invasive if there was >1 invasion strand within the ROI.

(7) For SP expression in mouse tumours, the mean fluorescence intensity for the entire ROI was measured. For SP expression levels in human breast tumours, fluorescence intensity was measured within an ROI drawn around any cancer-cell rich areas of the tumour. In all cases, multiple ROIs were measured per tumour, each dot in the plot corresponds to data from a single ROI. *r* represents independent tumours.

(8) For SLIT2 expression analysis within the tumour endothelium, the mean fluorescence intensity for SLIT2 along the endothelium (marked by endomucin) was measured. Multiple ROIs were measured per tumour, each dot in the plot corresponds to data from a single ROI. *r* represents independent tumours.

(9) NucView 488 caspase-3 substrate (Biotium, 30029-T) was used to visualize apoptosis within spheroids. The green fluorescence was used to measure the apoptotic area (thresholded in ImageJ) and a manually traced spheroid boundary was used to measure the total area.

(10) Calcium imaging was performed using the Fluo-4 calcium dye[71] (excitation 488 nm/emission 525 nm; Thermo Fisher Scientific, F14201). DRG neurons were cultured on a collagen I layer either alone or in the presence of 67NR cancer cells for at least 48 h before loading with the calcium dye. Cells were incubated with Fluo-4 (5 µM) for 60 min at 37 °C. Neurons were washed three times, and the medium was replaced with the BrainPhys Imaging Optimized Medium (StemCell Technologies, 05796). Live-cell imaging was performed for around 1 h to capture spontaneous calcium spikes using the Nikon TiE inverted microscope with Perfect Focus mechanism. Images were collected every 3–5 s. Imaris (v.10) was used to measure the mean fluorescence intensity within the soma of neurons within each ROI, at each timepoint. A rolling baseline was defined as the tenth percentile of the fluorescence intensity every 35 image frames. $\Delta F/F_0$ values are represented in the heat map (Fig. 3b) and individual calcium traces (Extended Data Fig. 7c).

Statistical analysis

For all experiments, independent biological replicates are listed as *r* values. For 3D invasion/proliferation assays used in the study, each dot in the plot represents quantification for a single spheroid/organoid (or *n*). Groups were compared using tests for significance as indicated in the figure legends. $P < 0.05$ was considered to be significant. Unless noted otherwise, all data are expressed as mean ± s.d. and all statistical tests were two-sided.

RNA-sequencing analysis

Libraries were constructed from 500 ng of total RNAs isolated from 4T1 (scrambled versus *Tlr7* shRNA) using the TruSeq RNA Library Prep Kit (Illumina). Constructed libraries were sequenced using the Illumina NextSeq (High Output, 75 SR) system at the Rockefeller University Genomics Center. Sequencing reads were mapped to the mouse genome (assembly GRCm38) using STAR aligner (v.2.7.5) using the default settings. STAR was also used for counting reads mapping to genes. Further analyses were performed using RStudio (v.4.1.0). Differentially expressed genes were determined using DESeq2 (v.1.32.0). For GSEA, genes were ranked according to log-transformed fold changes shrunken using the 'ashr' method and enriched pathways of the KEGG database were identified using the 'gseKEGG' function of the clusterProfiler package for RStudio (v.4.0.0).

Analysis of the TCGA and METABRIC studies

To assess the association of TLR7-dependent signalling with outcome in patients with breast cancer, we analysed the association of a TLR7-dependent (orthologous to human TLR8) gene signature with survival in two large independent datasets. Specifically, we generated a signature of genes downregulated in cancer spheroids in which *Tlr7* expression was silenced (see the section above) and calculated the TLR7 signature score by summing the scaled expression of the genes contained in the signature and using the ranked signature score as a covariate in a Cox proportional hazards model that included tumour stage, age and the ranked signature score using the Survival (v.3.2-11)

and forestmodel (v.0.6.2) packages for RStudio. For the TCGA study, we used clinical data as recently curated and included only primary tumour samples. For the METABRIC[72] study, we used the validation cohort.

Reporting summary

Further information on research design is available in the Nature Portfolio Reporting Summary linked to this article.

Data availability

Raw sequencing data and count tables for transcriptional profiling of 4T1-derived spheroids have been deposited at the Gene Expression Omnibus under accession number GSE267958. Reads were mapped to the mouse genome assembly GRCm38. Data for the METABRIC study are publicly available under EGA accession number EGAS00000000083. Data from the TCGA study are publicly available online (https://portal.gdc.cancer.gov). Source data are provided with this paper.

Code availability

All custom computer code is publicly available at GitHub (https://github.com/benostendorf/padmanaban_etal_2024).

51. Cao, Y. Q. et al. Primary afferent tachykinins are required to experience moderate to intense pain. *Nature* **392**, 390–394 (1998).
52. Wang, Y. et al. Ephrin-B2 controls VEGF-induced angiogenesis and lymphangiogenesis. *Nature* **465**, 483–486 (2010).
53. Guy, C. T., Cardiff, R. D. & Muller, W. J. Induction of mammary tumors by expression of polyomavirus middle T oncogene: a transgenic mouse model for metastatic disease. *Mol. Cell. Biol.* **12**, 954–961 (1992).
54. Maroulakou, I. G., Anver, M., Garrett, L. & Green, J. E. Prostate and mammary adenocarcinoma in transgenic mice carrying a rat C3(1) simian virus 40 large tumor antigen fusion gene. *Proc. Natl Acad. Sci. USA* **91**, 11236–11240 (1994).
55. Hale, J. J. et al. Structural optimization affording 2-(*R*)-(1-(*R*)-3, 5-bis(trifluoromethyl) phenylethoxy)-3-(S)-(4-fluoro)phenyl-4- (3-oxo-1,2,4-triazol-5-yl)methylmorpholine, a potent, orally active, long-acting morpholine acetal human NK-1 receptor antagonist. *J. Med. Chem.* **41**, 4607–4614 (1998).
56. Padmanaban, V. et al. Organotypic culture assays for murine and human primary and metastatic-site tumors. *Nat. Protoc.* **15**, 2413–2442 (2020).
57. Young, L., Sung, J., Stacey, G. & Masters, J. R. Detection of Mycoplasma in cell cultures. *Nat. Protoc.* **5**, 929–934 (2010).
58. Foty, R. A simple hanging drop cell culture protocol for generation of 3D spheroids. *J. Vis. Exp.* https://doi.org/10.3791/2720 (2011).
59. Heil, F. et al. Species-specific recognition of single-stranded RNA via Toll-like receptor 7 and 8. *Science* **303**, 1526–1529 (2004).
60. Alexopoulou, L., Holt, A. C., Medzhitov, R. & Flavell, R. A. Recognition of double-stranded RNA and activation of NF-κB by Toll-like receptor 3. *Nature* **413**, 732–738 (2001).
61. Hemmi, H. et al. Small anti-viral compounds activate immune cells via the TLR7 MyD88-dependent signaling pathway. *Nat. Immunol.* **3**, 196–200 (2002).
62. Jurk, M. et al. Human TLR7 or TLR8 independently confer responsiveness to the antiviral compound R-848. *Nat. Immunol.* **3**, 499 (2002).
63. Maira, S. M. et al. Identification and characterization of NVP-BKM120, an orally available pan-class I PI3-kinase inhibitor. *Mol. Cancer Ther.* **11**, 317–328 (2012).
64. Davies, B. R. et al. Preclinical pharmacology of AZD5363, an inhibitor of AKT: pharmacodynamics, antitumor activity, and correlation of monotherapy activity with genetic background. *Mol. Cancer Ther.* **11**, 873–887 (2012).
65. Folkes, A. J. et al. The identification of 2-(1*H*-indazol-4-yl)-6-(4-methanesulfonyl-piperazin-1-ylmethyl)-4-morpholin-4-yl-thieno[3,2-*d*]pyrimidine (GDC-0941) as a potent, selective, orally bioavailable inhibitor of class I PI3 kinase for the treatment of cancer. *J. Med. Chem.* **51**, 5522–5532 (2008).
66. Padmanaban, V. et al. E-cadherin is required for metastasis in multiple models of breast cancer. *Nature* **573**, 439–444 (2019).
67. Krause, S., Brock, A. & Ingber, D. E. Intraductal injection for localized drug delivery to the mouse mammary gland. *J. Vis. Exp.* https://doi.org/10.3791/50692 (2013).
68. Jancso, G., Kiraly, E., Such, G., Joo, F. & Nagy, A. Neurotoxic effect of capsaicin in mammals. *Acta Physiol. Hung.* **69**, 295–313 (1987).
69. Chi, J. et al. Three-dimensional adipose tissue imaging reveals regional variation in beige fat biogenesis and PRDM16-dependent sympathetic neurite density. *Cell Metab.* **27**, 226–236 (2018).
70. Luppi, P. H., Fort, P. & Jouvet, M. Iontophoretic application of unconjugated cholera toxin B subunit (CTb) combined with immunohistochemistry of neurochemical substances: a method for transmitter identification of retrogradely labeled neurons. *Brain Res.* **534**, 209–224 (1990).
71. Gee, K. R. et al. Chemical and physiological characterization of fluo-4 Ca^{2+}-indicator dyes. *Cell Calcium* **27**, 97–106 (2000).
72. Curtis, C. et al. The genomic and transcriptomic architecture of 2,000 breast tumours reveals novel subgroups. *Nature* **486**, 346–352 (2012).

Acknowledgements We thank the members of our laboratory for discussions and feedback on the manuscript text; P. Rajasethupathy for advice on calcium imaging analysis; M. Klatt for technical help with several animal experiments; the members of the various resource centres at Rockefeller University, including A. North, C. Pyrgaki, Banerjee P., and other staff of the Bio Imaging Resource Center, including C. Zhao, the staff of the Genomics Resource Center, S. Mazel and the staff of the Flow Cytometry Resource Center. The results published here are in part based on data generated by the TCGA Research Network. This work was supported by U54CA261701, R35CA274446, the Black Family Metastasis Center, the Breast Cancer Research Foundation and the Reem Kayden award. V.P. was supported by the Hope Funds for Cancer Research postdoctoral fellowship. I.K. is member of the German Academic Scholarship Foundation (Studienstiftung des deutschen Volkes) and was awarded a fellowship from Boehringer Ingelheim Fonds (BIF). B.N.O. was supported by a Max Eder grant of the German Cancer Aid (70114327) and is a fellow of the digital clinician scientist program at BIH-Charité.

Author contributions V.P. and S.F.T. conceptualized the study, designed experiments, supervised research and wrote the manuscript with input from all of the authors. V.P. performed most of the experiments with technical assistance from I.K., E.S.S. and Z.K.; B.N.O. analysed mRNA-sequencing data. S.F.T. obtained funding and supervised scientists.

Competing interests The authors declare no competing interests.

Additional information
Supplementary information The online version contains supplementary material available at https://doi.org/10.1038/s41586-024-07767-5.

Correspondence and requests for materials should be addressed to Sohail F. Tavazoie.

Peer review information *Nature* thanks Osamu Takeuchi and the other, anonymous, reviewer(s) for their contribution to the peer review of this work. Peer reviewer reports are available.

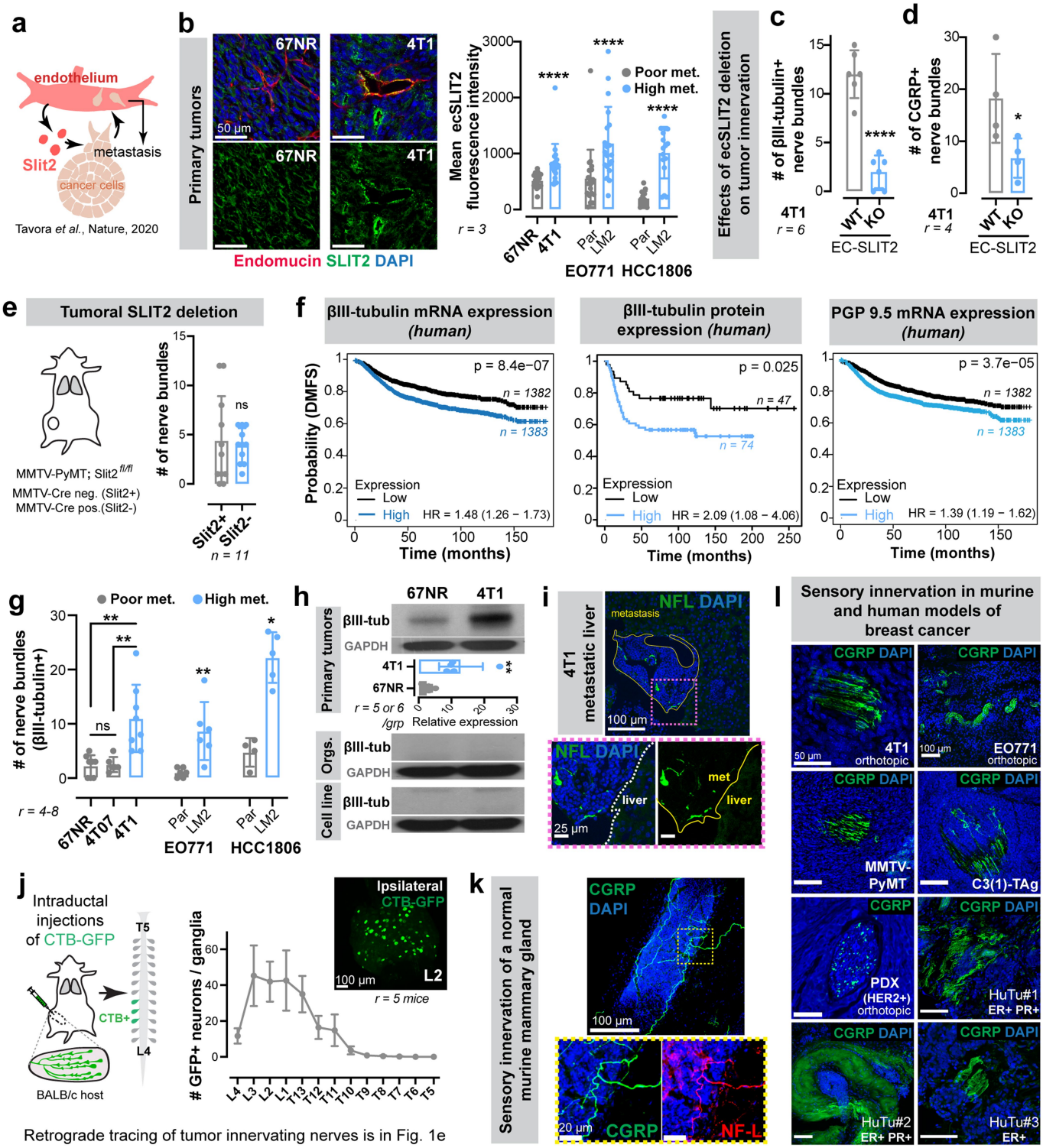

Extended Data Fig. 1 | See next page for caption.

Extended Data Fig. 1 | Breast tumours are frequently innervated by sensory nerves. (a) We previously uncovered a requirement for endothelial-derived SLIT2 (ecSLIT2) in metastasis[15]. (b) Quantification of ecSLIT2 expression in poorly *vs* highly metastatic breast tumour models. ****$p < 0.0001$, Mann-Whitney test. Mean ± SD. (c-d) Quantification of total (c) and CGRP+ sensory (d) innervation in 4T1 tumours grown in ecSLIT2 knockout (endothelial-specific depletion of SLIT2) mice. **** $p < 0.0001$, *$p = 0.0489$, t-test. Mean ± SD. (e) Quantification of innervation in SLIT2-knockout mammary tumours in $Slit2^{fl/fl}$; MMTV-PyMT; MMTV-Cre mice. $^{ns}p = 0.6414$, Mann-Whitney test. Mean ± SD. (f) Kaplan-Meier plots showing distant metastasis-free survival (DMFS) of breast cancer patients sorted by the median expression level of βIII-tubulin (mRNA, protein) or PGP9.5 (mRNA) of their tumours. The x-axes were set to have >10 surviving patients in each arm. (g) Nerve bundle abundance in highly metastatic primary tumours relative to corresponding isogenic poorly metastatic tumours. Between 4 and 8 tumours were analysed per group. $^{**}p$ (67NR vs 4T1) = 0.001, $^{**}p$ (4T07 vs 4T1) = 0.0019, ^{ns}p (67NR vs 4T07) = 0.9095, ANOVA; $^{**}p$ (EO771 Par vs LM2) = 0.0065, $^{*}p$ (HCC1806 Par vs LM2) = 0.0159, Mann-Whitney test. Mean ± SD. (h) Expression of pan-neuronal βIII-tubulin in 67NR *vs* 4T1 primary tumours, stroma-depleted primary tumour organoids, or cell lines. $^{**}p = 0.0048$, t-test. Mean ± SD. MW: βIII-tubulin (50 kDa). (i) Liver metastasis from a 4T1 tumour-bearing mouse immuno-stained for nerve fibres. $r = 3$/group. (j) Retrograde tracing of DRG neurons innervating abdominal mammary glands of wild-type mice. Mean ± SEM. (k-l) Sensory, CGRP+ innervation observed within the normal murine mammary gland (k), murine models of breast cancer (l), and primary human tumours (l). $r = 3$ tumours/ group.

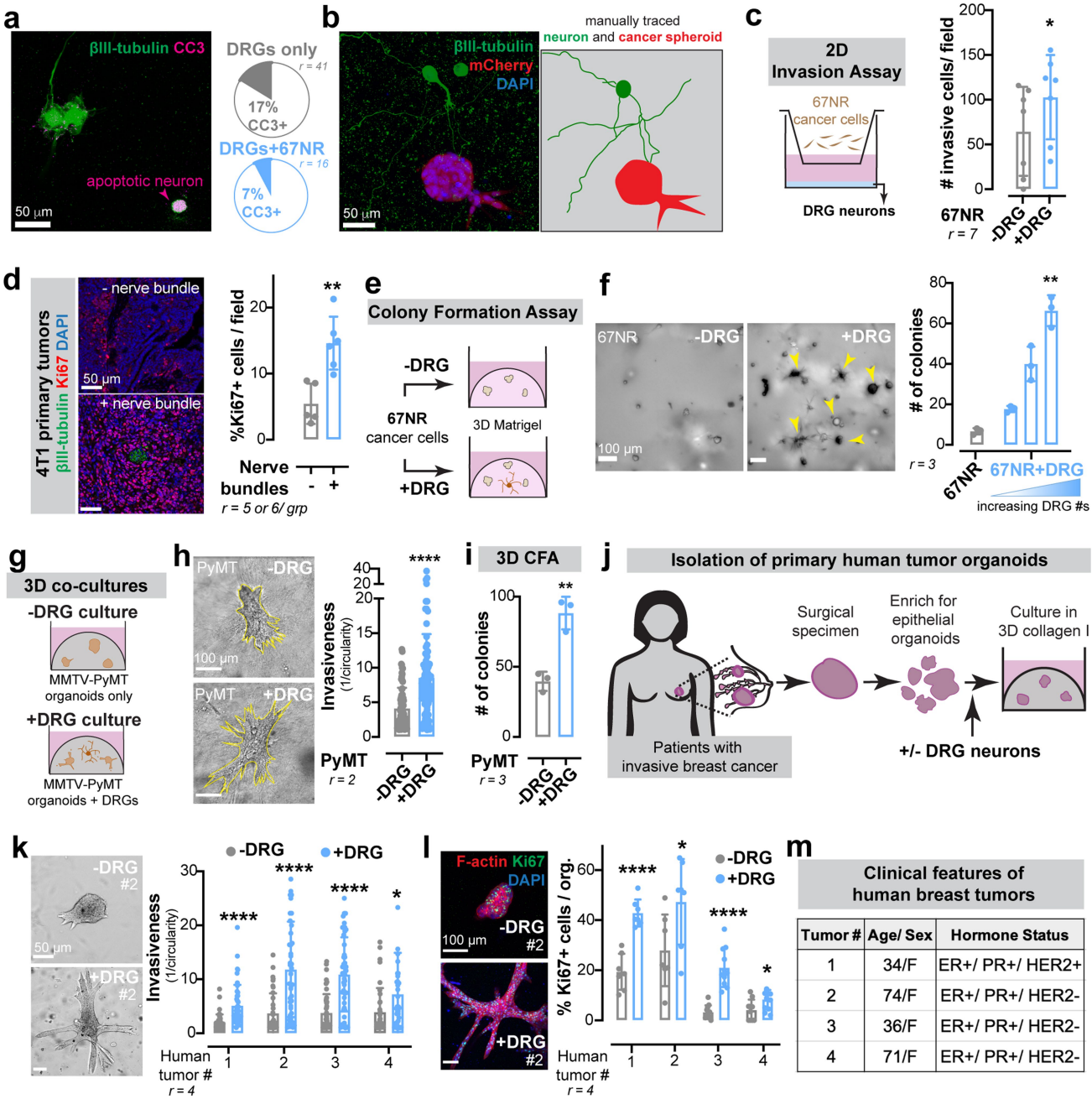

Tumor #	Age/ Sex	Hormone Status
1	34/F	ER+/ PR+/ HER2+
2	74/F	ER+/ PR+/ HER2-
3	36/F	ER+/ PR+/ HER2-
4	71/F	ER+/ PR+/ HER2-

Extended Data Fig. 2 | Sensory neurons promote cancer invasion and proliferation across multiple ex vivo murine and human models of breast cancer. (a) Frequency of apoptosis (cleaved caspase 3, CC3 +) in DRG neurons cultured alone or in the presence of 67NR cancer cells. (b) Micrographs of mCherry+ 67NR spheroids co-cultured with βIII-tubulin+ DRG neurons. Neuron and spheroid boundaries are manually traced to illustrate little physical contact. $n = 10$ ROIs/ group, $r = 4$. (c) 2D invasion assay of 67NR cancer cells that were cultured alone or in the presence of primary DRG neurons. $^{*}p = 0.0432$, t-test. Mean ± SD. (d) Quantification of the number of mitotically active cells within regions of 4T1 primary tumours adjacent to or far away from a nerve bundle. $^{**}p = 0.0043$, Mann-Whitney test. Mean ± SD. (e-f) 3D colony formation assay. 67NR cancer cells were cultured alone or in the presence of DRG neurons in 3D Matrigel. (e) Schematic. (f) Quantification. $^{**}p = 0.0067$, Kruskal-Wallis test. Mean ± SD. (g-i) 3D co-culture assays of MMTV-PyMT mammary tumour organoids and primary DRG neurons. (g) Schematic. (h) Invasion assay. $^{****}p < 0.0001$, Mann-Whitney test. (i) Colony formation assay. $^{**}p = 0.0033$, t-test. Mean ± SD. (j-m) 3D co-culture assays of 4 independent primary human breast tumours and DRG neurons. (j) Schematic of organoid isolation. (k) Invasion quantification. $^{****}p < 0.0001$, $^{*}p = 0.0266$, Mann-Whitney test. Mean ± SD. (l) Proliferation quantification. $^{****}p < 0.0001$, $^{*}p = 0.0401$ (#2), 0.0267 (#4), t-test. Mean ± SD. (m) Basic de-identified clinical information for human tumour samples cultured.

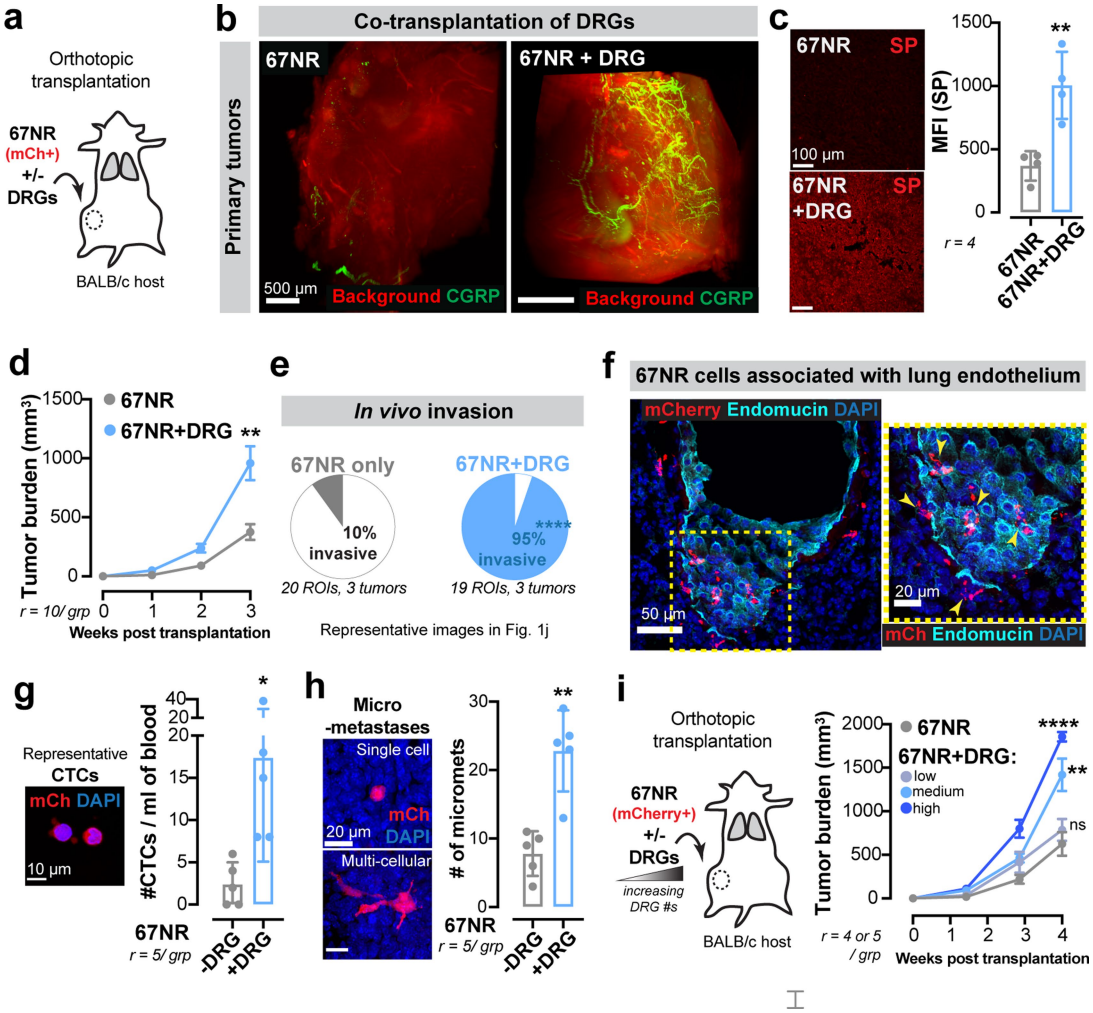

Extended Data Fig. 3 | Co-transplantation of breast cancer cells with DRG neurons drives metastasis. (a-h) Co-transplantation of mCherry+ (mCh) 67NR cancer cells and DRG neurons. (a) Schematic. (b) Optically cleared 67NR tumours transplanted with or without DRG neurons and immunostained for CGRP+ sensory nerves. $r = 2$ tumours/ group. (c) Mean fluorescence intensity (MFI) for SP in 67NR primary tumours transplanted with or without DRG neurons. $^{**}p = 0.0046$, t-test. Mean ± SD. (d) Tumour growth. $^{**}p = 0.0017$, t-test. Mean ± SEM. (e) Percentage of the tumour-stroma boundary with a pushing *vs* invasive morphology. $^{****}p < 0.0001$, Chi-square test. (f) Association of mCh+ 67NR cancer cells with the lung endothelium in mice transplanted with orthotopic 67NR tumours. $r = 3$ lungs/ group. (g) CTC enumeration in mice transplanted with mCh+ 67NR cancer cells with or without DRG neurons. $^{*}p = 0.0287$, t-test. Mean ± SD. (h) mCh+ micro-metastases. $^{**}p = 0.0079$, Mann-Whitney test. Mean ± SD. (i) Co-transplantation of 67NR cancer cells with increasing numbers of DRG neurons. $^{ns}p = 0.4124$, $^{**}p = 0.0026$, $^{****}p < 0.0001$, ANOVA. Mean ± SEM.

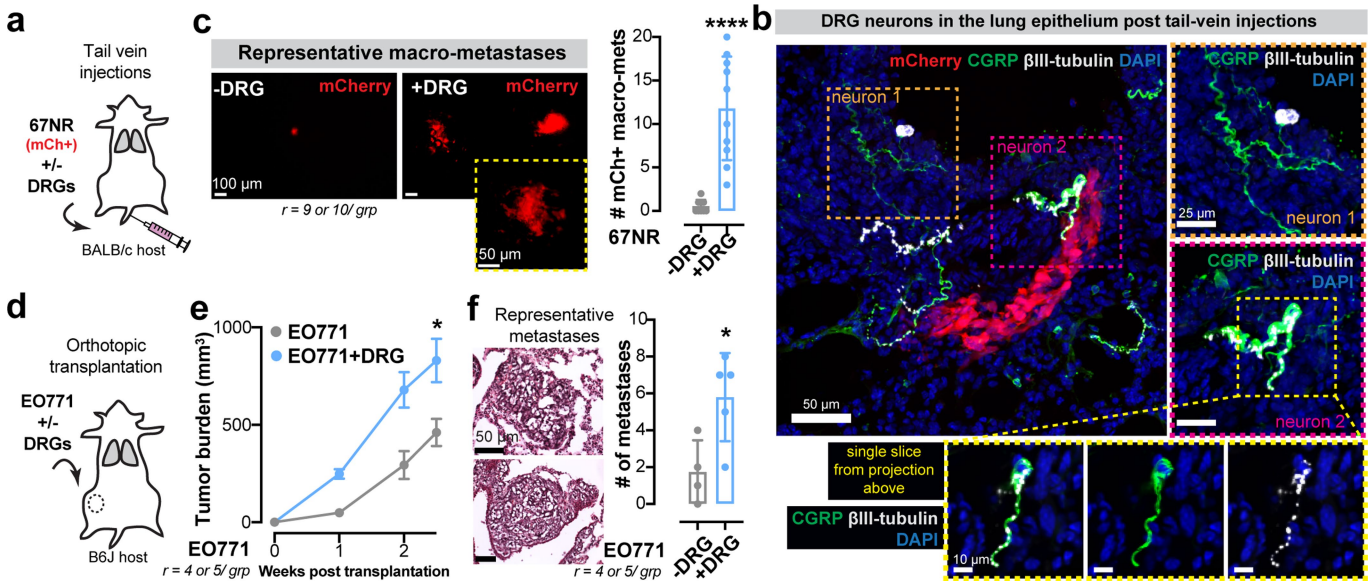

Extended Data Fig. 4 | Sensory neurons drive metastatic colonization in multiple breast cancer models. (a-c) Tail vein injections of mCh+ 67NR cancer cells with or without DRG neurons. (a) Schematic. (b) CGRP + / βIII-tubulin+ neuronal cell bodies in mice co-injected with DRG neurons. $r = 3$ lungs/ group. (c) mCh+ metastases. ****$p < 0.0001$, Mann-Whitney test. Mean ± SD. (d-f) Co-transplantation of EO771 cancer cells and DRG neurons. (d) Schematic. (e) Tumour growth. *$p = 0.0345$, t-test. Mean ± SEM. (f) Number of micro-metastases counted by H&E. *$p = 0.0249$, t-test. Mean ± SD.

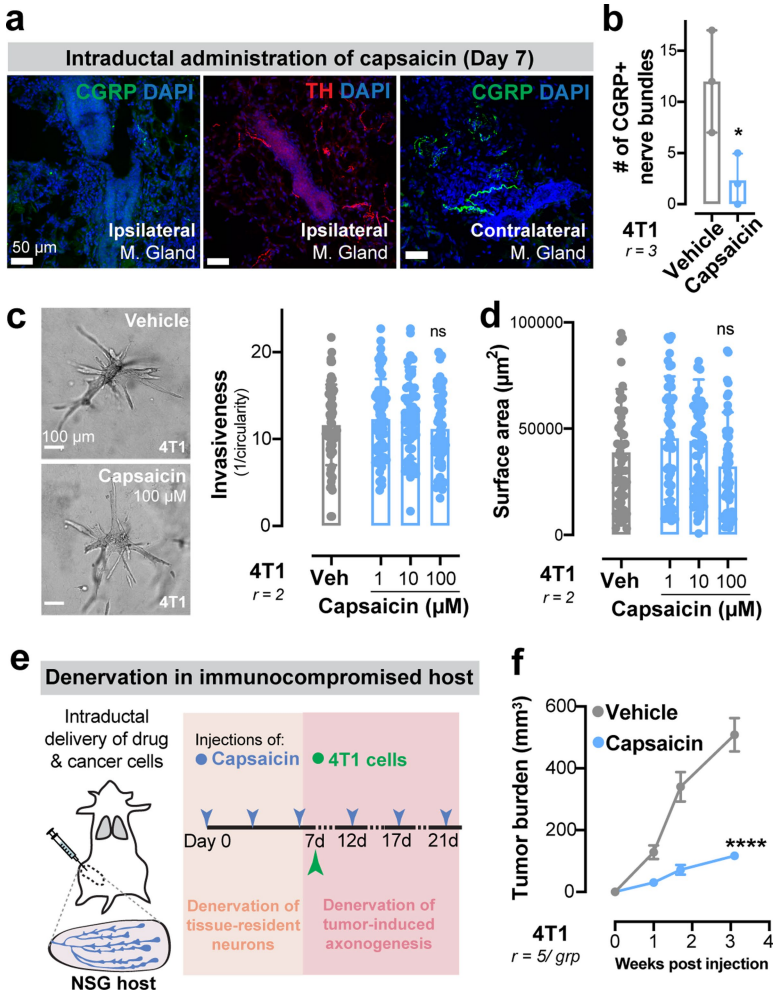

Extended Data Fig. 5 | Capsaicin does not alter growth or invasion of cancer cells in vitro and reduces tumour growth in immune-compromised mice in vivo. (a) Sensory (CGRP +) and sympathetic (TH +) innervation in ipsilateral or contralateral mammary glands 7 days after capsaicin administration. (b) Quantification of CGRP+ nerve bundles post-capsaicin administration. *$p = 0.0403$, t-test. Mean ± SD. (c-d) 3D culture of 4T1 spheroids in the presence of capsaicin (1–100 µM). (c) Invasion quantification. $^{ns}p > 0.9999$, Kruskal-Wallis test. (d) Spheroid surface area. $^{ns}p = 0.7108$, Kruskal-Wallis test. Mean ± SD. (e-f) Sensory-specific denervation of 4T1 tumours grown in NSG mice. (e) Schematic. (f) Tumour growth. ****$p < 0.0001$, t-test. Mean ± SEM.

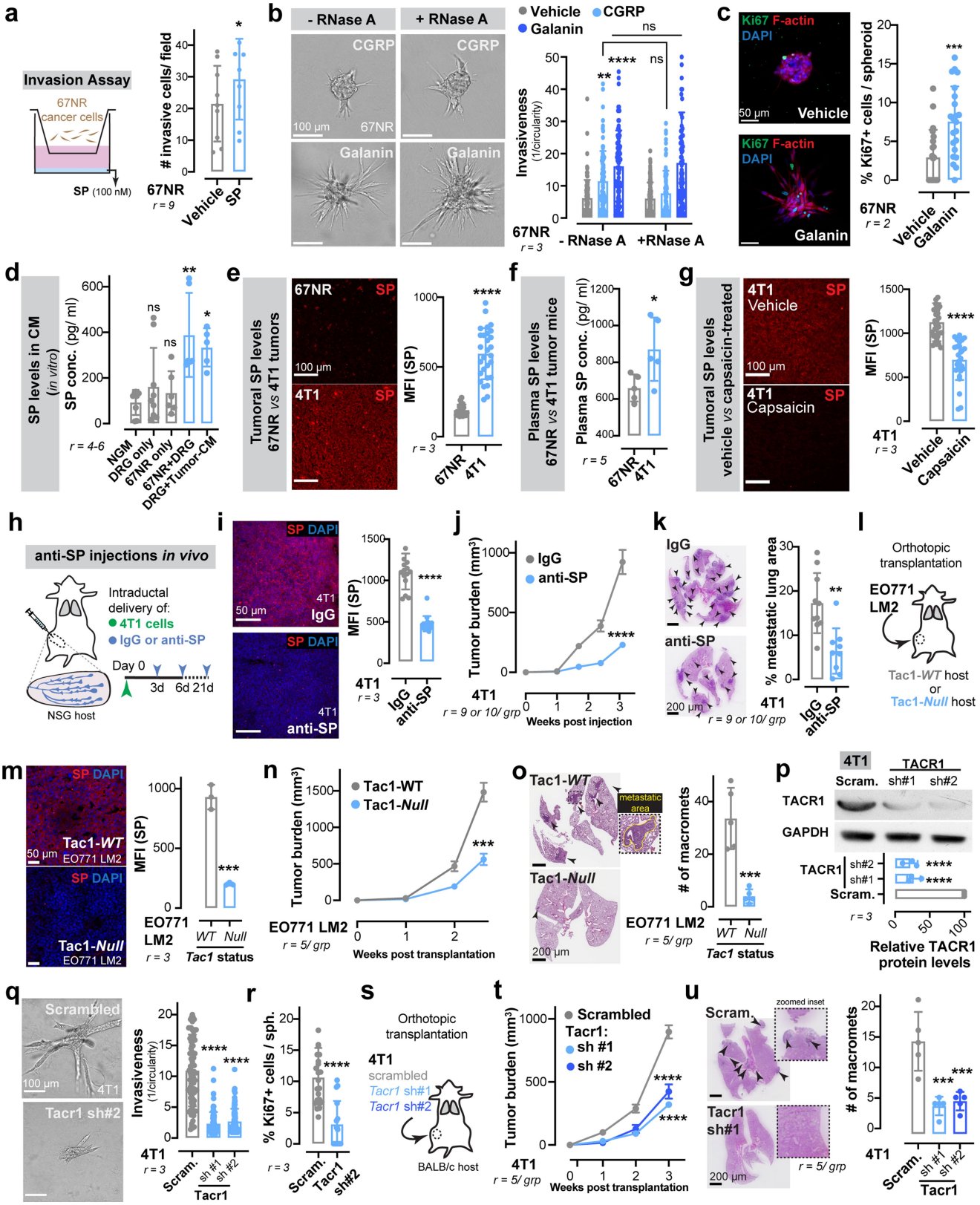

Extended Data Fig. 6 | See next page for caption.

Extended Data Fig. 6 | Neuronal substance-P drives breast cancer metastasis via the activation of the tumoral TACR1 receptor. (a) Invasion assay of 67NR cancer cells in response to SP. *p = 0.0254, t-test. Mean ± SD. (b-c) 67NR cancer cell spheroids cultured with neuropeptides galanin or CGRP, with or without RNase A. (b) Invasion quantification. **p = 0.0011, ****p < 0.0001, ^{ns}p (CGRP) = 0.1066, ^{ns}p (galanin) > 0.9999, Kruskal-Wallis test. Vehicle-treated 67NR spheroids (−/+RNase A) are also plotted in Fig. 2d and Fig. 3d respectively since the experiments were conducted together. (c) Proliferation quantification. ***p = 0.0006, Mann-Whitney test. Mean ± SD. (d) ELISA-based quantification for SP levels in conditioned medium. p values are based on comparisons with base medium (NGM). ^{ns}p = 0.7426 (*vs* DRG only), 0.8724 (*vs* 67NR only); *p = 0.0213; **p = 0.0024, ANOVA. Mean ± SD. (e-g) In vivo measurements of SP expression. (e) Mean fluorescence intensity (MFI) of SP in 4T1 *vs* 67NR primary tumours. ****p < 0.0001, t-test. (f) Plasma SP levels in 67NR *vs* 4T1 tumour-bearing mice. *p = 0.0359, t-test. (g) MFI of SP in 4T1 vehicle *vs* capsaicin-treated primary tumours. ****p < 0.0001, t-test. Mean ± SD. (h-k) Effects of an SP-blocking antibody on 4T1 tumour growth and metastasis. (h) Schematic. (i) MFI of SP in IgG *vs* anti-SP treated 4T1 tumours. ****p < 0.0001, Mann-Whitney test. Mean ± SD. (j) Tumour growth. ****p < 0.0001, Mann-Whitney test. Mean ± SEM. (k) Metastatic area quantified by H&E. **p = 0.0012, t-test. Mean ± SD. (l-o) Orthotopic transplantation of EO771 LM2 cells into the abdominal mammary glands of *Tac1-WT* and *Tac1-null* host mice. (l) Schematic. (m) MFI of SP in primary tumours. ***p = 0.0003, t-test. Mean ± SD. (n) Tumour growth. ***p = 0.0003, t-test. Mean ± SEM. (o) Number of macro-metastases quantified by H&E. ***p = 0.0006, t-test. Mean ± SD. (p-r) Depletion of SP's receptor, TACR1 in 4T1 cancer cell spheroids. (p) Validation of knockdown. ****p < 0.0001, ANOVA. MW: TACR1 (46 kDa). Quantification of spheroid invasion (q) and proliferation (r). ****p < 0.0001, Mann-Whitney test. Mean ± SD. (s-u) Orthotopic transplantation of 4T1 cancer cells depleted for TACR1. (s) Schematic. (t) Tumour growth. ****p < 0.0001, ANOVA. Mean ± SEM. (u) Metastatic area quantified by H&E. ***p = 0.0003, ANOVA. Mean ± SD.

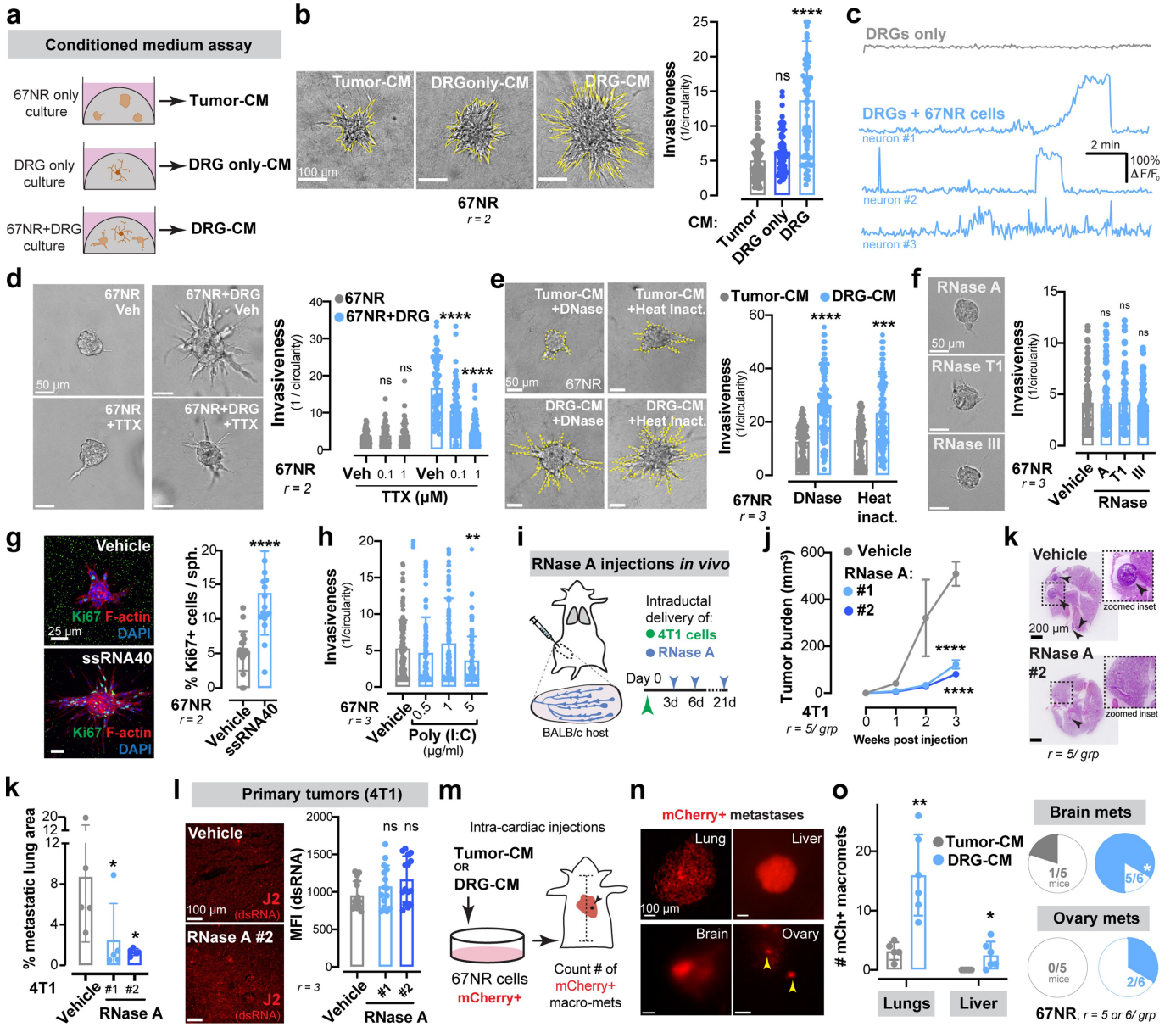

Extended Data Fig. 7 | Neuronal SP drives metastasis in a ssRNA-dependent manner. (a-b) Schematic for isolation of conditioned medium from tumour only, DRG only, or tumour-DRG cultures (a). Invasion quantification, $^{ns}p = 0.1463$, $^{****}p < 0.0001$, Kruskal-Wallis test (b). Mean ± SD. (c) Calcium fluorescence traces ($\Delta F/F_0$) of DRG neurons cultured alone or in the presence of 67NR cancer cells. F = measured fluorescence, F_0 = baseline fluorescence. (d) Invasion quantification of 67NR spheroids co-cultured with DRG neurons in the presence of a sodium channel blocker, tetrodotoxin (TTX). $^{ns}p > 0.9999$, $^{****}p < 0.0001$, Kruskal-Wallis test. Mean ± SD. (e) Invasion quantification of 67NR spheroids cultured with DNase-treated or heat inactivated tumour-CM or DRG-CM. $^{***}p = 0.001$, $^{****}p < 0.0001$, Kruskal-Wallis test. Mean ± SD. (f) Invasion quantification of 67NR spheroids cultured with solely RNase A, RNase T1 or RNase III. $^{ns}p > 0.9999$, Kruskal-Wallis test. Mean ± SD. (g) Proliferation quantification of 67NR spheroids cultured with or without ssRNA40. $^{****}p < 0.0001$, Mann-Whitney test. Mean ± SD. (h) Invasion quantification of 67NR spheroids cultured with a dsRNA mimetic, Poly (I:C). $^{**}p = 0.0072$, Kruskal-Wallis test. Mean ± SD. (i-k) Effect of RNase A treatment on 4T1 tumour growth and metastasis. (i) Schematic. (j) Tumour growth. $^{****}p < 0.0001$, ANOVA. Mean ± SEM. (k) Metastatic area quantified by H&E. $^{*}p = 0.0392$ (vehicle *vs* RNase A #1), $^{*}p = 0.0347$ (vehicle *vs* RNase A #2), ANOVA. Mean ± SD. (l) MFI of dsRNA (measured using an anti-dsRNA antibody, J2) in vehicle *vs* RNase A treated 4T1 primary tumours. $^{ns}p = 0.22$ (RNase A #1), 0.0625 (RNase A #2), ANOVA. Mean ± SD. (m-o) Intra-cardiac injections of mCherry+ 67NR cancer cells pre-treated with tumour-CM or DRG-CM. (m) Schematic. (n) Representative mCherry+ metastases. (o) Quantification of mCherry+ metastases. $^{**}p = 0.0028$, $^{*}p = 0.0366$ (liver), $^{*}p = 0.0313$ (brain), t-test. Mean ± SD.

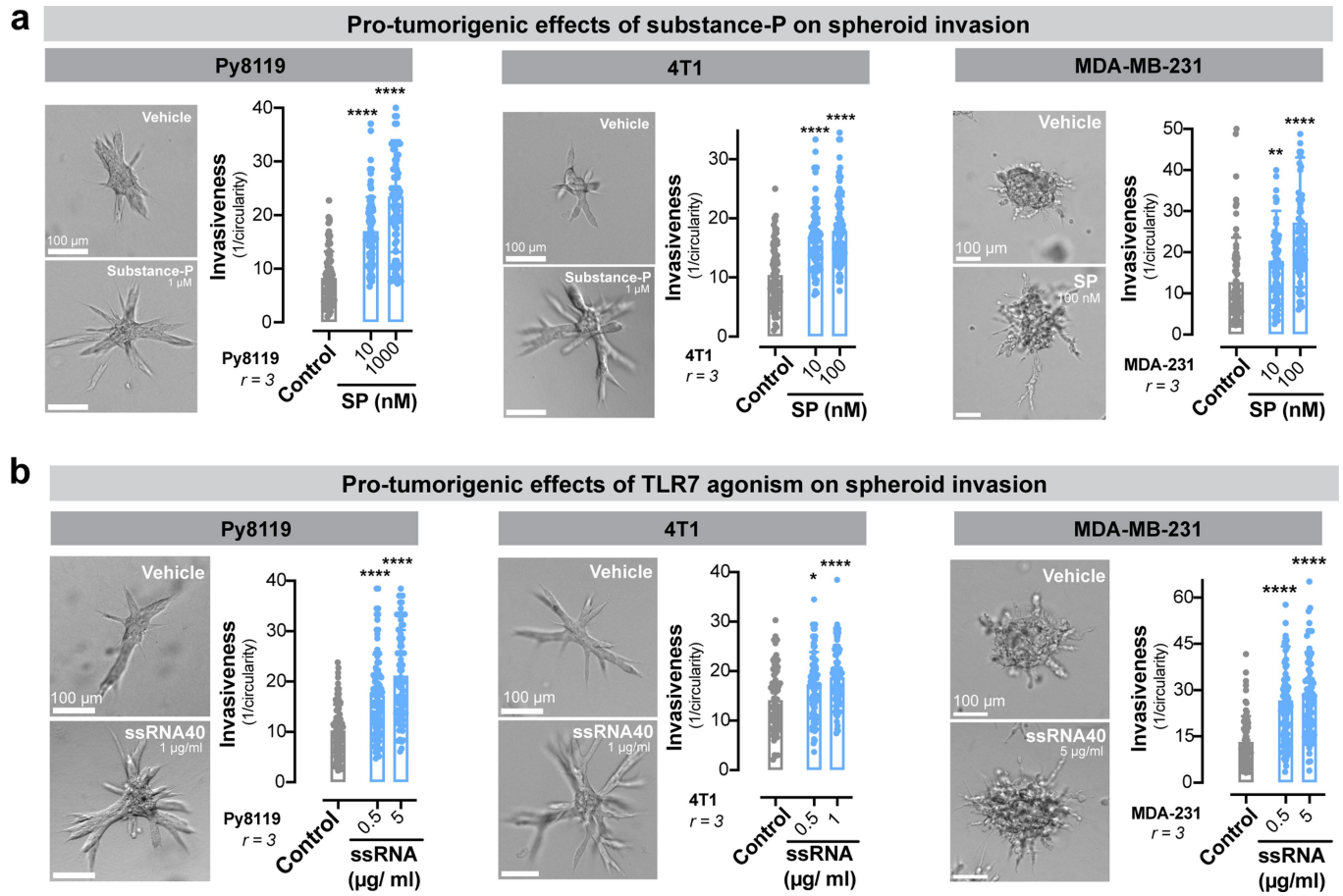

Extended Data Fig. 8 | SP-driven activation of TACR1 and ssRNA-driven activation of TLR7 promote breast cancer invasiveness across multiple models of breast cancer. (a) Invasion quantification of Py8119, 4T1, and MDA-MB-231 breast cancer spheroids in the presence of SP. $^{**}p = 0.0013$, $^{****}p < 0.0001$, Kruskal-Wallis test. Mean ± SD. (b) Invasion quantification of Py8119, 4T1, and MDA-MB-231 breast cancer spheroids in the presence of ssRNA40. $^{*}p = 0.0235$, $^{****}p < 0.0001$, Kruskal-Wallis test. Mean ± SD.

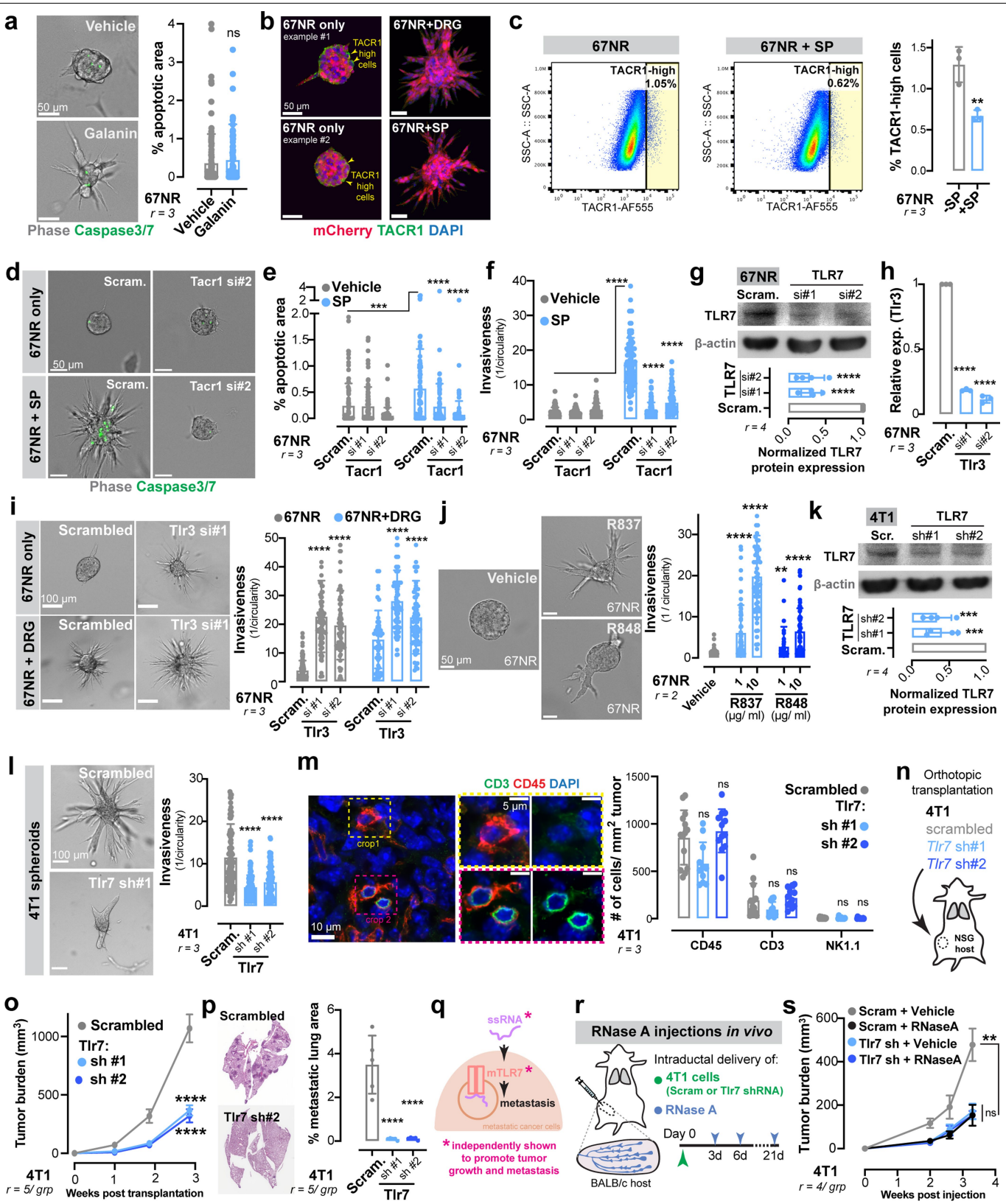

Extended Data Fig. 9 | See next page for caption.

Extended Data Fig. 9 | Neuronal SP signals via tumoral TLR7 receptors to drive metastasis. (a) Percent apoptotic area within 67NR spheroids cultured with galanin. $^{ns}p = 0.0807$, Mann-Whitney test. Mean ± SD. (b) 67NR spheroids cultured with or without DRG neurons and immunostained for TACR1. $n = 10$ spheroids/ group. (c) Flow cytometry analysis of TACR1 expression in 67NR cancer cells. $^{**}p = 0.0089$, t-test. Mean ± SD. (d-f) 67NR spheroids depleted for TACR1 and cultured with SP. (e) Percent apoptotic area. $^{***}p = 0.0003$, Mann-Whitney test, $^{****}p < 0.0001$, Kruskal-Wallis test. (f) Invasion quantification. $^{****}p < 0.0001$, Kruskal-Wallis test. Mean ± SD. (g) Validation of *Tlr7* knockdown in 67NR cancer cells. $^{****}p < 0.0001$, ANOVA. Mean ± SD. MW: TLR7 (135 kDa). Validation of *Tlr3* knockdown in 67NR cancer cells. $^{****}p < 0.0001$, ANOVA. Mean ± SD. Invasion quantification of 67NR spheroids depleted for TLR3 and cultured with or without DRG neurons. $^{****}p < 0.0001$, Kruskal-Wallis test. Mean ± SD. Invasion quantification of 67NR spheroids cultured in the presence of TLR7 agonists, R837 or R848. $^{****}p < 0.0001$, $^{**}p = 0.0011$, Kruskal-Wallis test. Mean ± SD. Validation of *Tlr7* knockdown in 4T1 cancer cells. $^{***}p = 0.0006$, ANOVA. Mean ± SD. MW: TLR7 (135 kDa). Invasion quantification of 4T1 spheroids depleted of TLR7. $^{****}p < 0.0001$, Kruskal-Wallis test. Mean ± SD. Immunostaining for CD45 (all immune), CD3 (T cells), or NK1.1 (NK cells) on 4T1 primary tumours depleted of TLR7. $^{ns}p > 0.9999$ (all conditions), Kruskal-Wallis test. Mean ± SD. (n-p) Orthotopic transplantations of 4T1 cancer cells depleted for TLR7 in NSG mice. (n) Schematic. (o) Tumour growth. $^{****}p < 0.0001$, ANOVA. Mean ± SEM. (p) Metastatic area quantified by H&E. $^{****}p < 0.0001$, ANOVA. Mean ± SD. (q-s) Orthotopic transplantation of 4T1 cancer cells depleted for TLR7, followed by periodic injections of RNase A. (q,r) Schematics. (s) Tumour growth. $^{**}p = 0.0033$, $^{ns}p = 0.9923$, ANOVA. Mean ± SD.

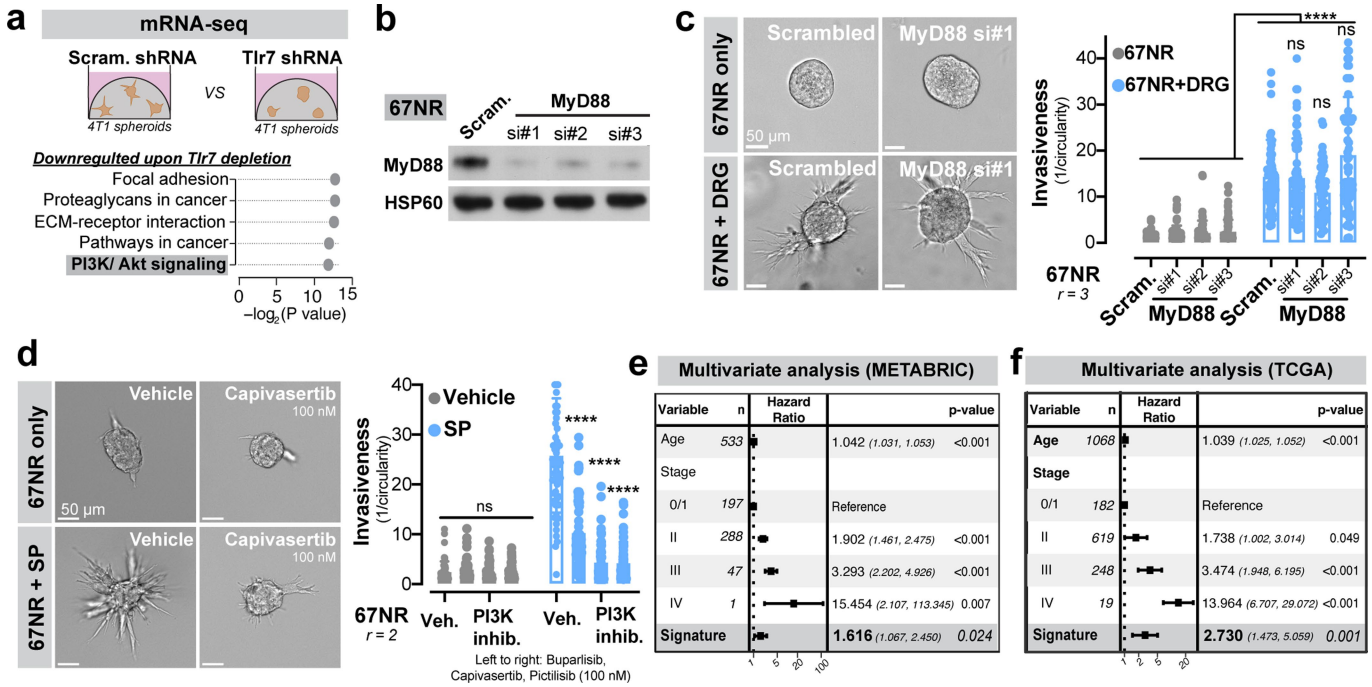

Extended Data Fig. 10 | Sensory neurons activate a non-canonical TLR7 signalling axis in cancer cells which correlates with poor patient outcome. (a) mRNA sequencing of control *vs Tlr7* depleted 4T1 spheroids. Top five downregulated pathways in 4T1 spheroids depleted for *Tlr7* as assessed by gene set enrichment analysis (*p* values according to permutation testing). (b) Validation of MyD88 knockdown in 67NR cancer cells. MW: MyD88 (33 kDa). $r = 3$. (c) Invasion quantification of 67NR spheroids depleted for MyD88 and cultured with or without DRG neurons. $^{****}p < 0.0001$, Mann-Whitney test. $^{ns}p > 0.9999$ (si#1), $^{ns}p = 0.0783$ (si#2), $^{ns}p = 0.4140$ (si#3), Kruskal-Wallis test. Mean ± SD. (d) Invasion quantification of 67NR spheroids cultured with or without SP and a PI3K inhibitor (left to right: buparlisib, capivasertib, or pictilisib). ^{ns}p (Veh *vs* buparlisib) = 0.1273, ^{ns}p (Veh *vs* capivasertib) = 0.6967, ^{ns}p (Veh *vs* pictilisib) > 0.9999, $^{****}p < 0.0001$, Kruskal-Wallis test. Mean ± SD. (e-f) Multivariate analysis of the association of age, tumour stage and a *Tlr7*-dependent gene signature with survival in breast cancer patients from the METABRIC (e) and TCGA (f) datasets (*p* values according to multivariate Cox proportional hazard models, error bars indicate 95% confidence intervals).

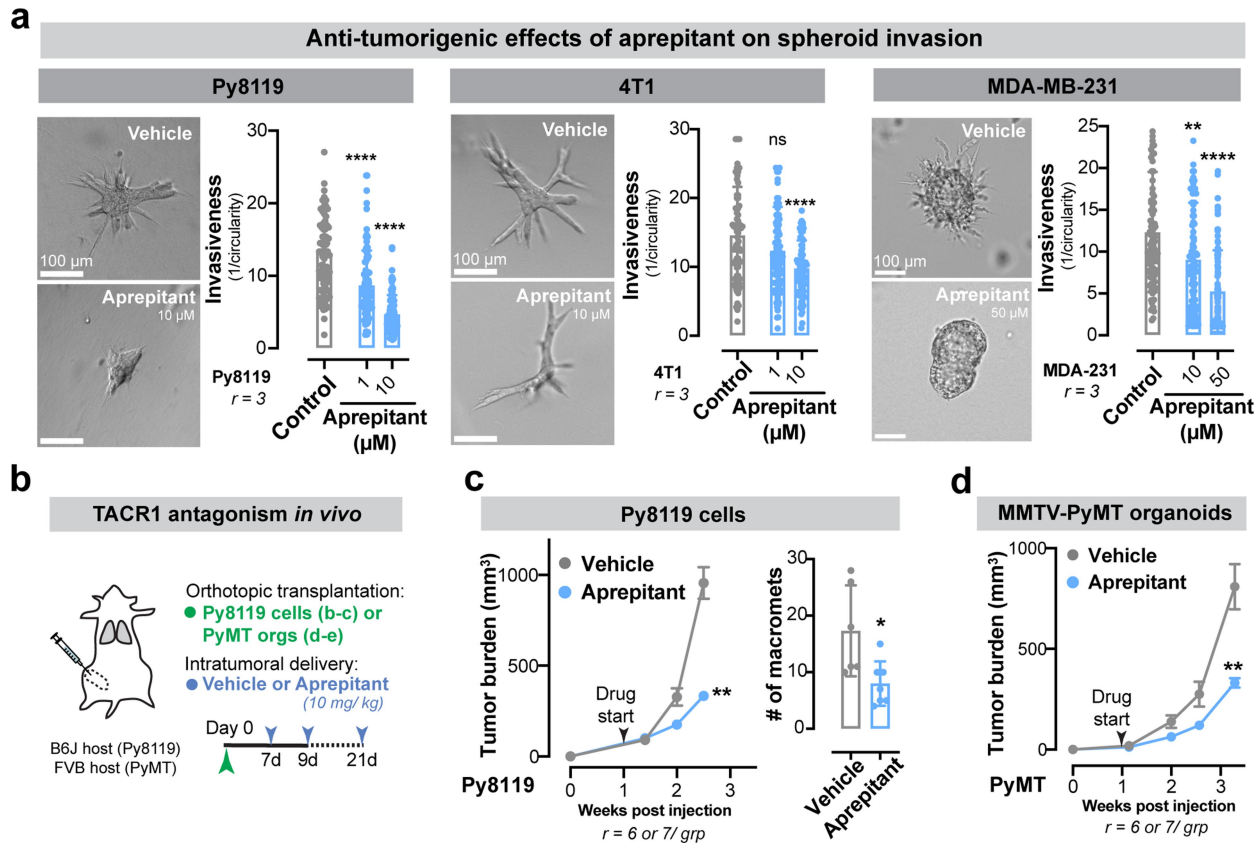

Extended Data Fig. 11 | Aprepitant impairs tumour growth and metastasis of Py8119 and MMTV-PyMT models of breast cancer. (a) Invasion quantification of Py8119, 4T1, and MDA-MB-231 breast cancer spheroids cultured in the presence of aprepitant. ****$p < 0.0001$, $^{ns}p = 0.9621$, **$p = 0.0013$, Kruskal-Wallis test. Mean ± SD. (b-d) Aprepitant was evaluated for its potential in inhibiting breast cancer progression and metastasis. (b) Schematic. (c) Py8119 tumour growth and metastasis count. **$p = 0.0012$, *$p = 0.0117$, Mann-Whitney test. (d) MMTV-PyMT tumour growth. **$p = 0.0047$, Mann-Whitney test. Mean ± SEM.

nature portfolio

Corresponding author(s): Sohail Tavazoie

Last updated by author(s): Jun 10, 2024

Reporting Summary

Nature Portfolio wishes to improve the reproducibility of the work that we publish. This form provides structure for consistency and transparency in reporting. For further information on Nature Portfolio policies, see our Editorial Policies and the Editorial Policy Checklist.

Statistics

For all statistical analyses, confirm that the following items are present in the figure legend, table legend, main text, or Methods section.

n/a | Confirmed

- [x] The exact sample size (*n*) for each experimental group/condition, given as a discrete number and unit of measurement
- [x] A statement on whether measurements were taken from distinct samples or whether the same sample was measured repeatedly
- [x] The statistical test(s) used AND whether they are one- or two-sided
  Only common tests should be described solely by name; describe more complex techniques in the Methods section.
- [x] A description of all covariates tested
- [x] A description of any assumptions or corrections, such as tests of normality and adjustment for multiple comparisons
- [x] A full description of the statistical parameters including central tendency (e.g. means) or other basic estimates (e.g. regression coefficient) AND variation (e.g. standard deviation) or associated estimates of uncertainty (e.g. confidence intervals)
- [x] For null hypothesis testing, the test statistic (e.g. *F*, *t*, *r*) with confidence intervals, effect sizes, degrees of freedom and *P* value noted
  Give P values as exact values whenever suitable.
- [x] For Bayesian analysis, information on the choice of priors and Markov chain Monte Carlo settings
- [x] For hierarchical and complex designs, identification of the appropriate level for tests and full reporting of outcomes
- [x] Estimates of effect sizes (e.g. Cohen's *d*, Pearson's *r*), indicating how they were calculated

Our web collection on statistics for biologists contains articles on many of the points above.

Software and code

Policy information about availability of computer code

Data collection	No custom or open-sourced software was used for data collection
Data analysis	Analysis of previously published whole-exome sequencing data (TCGA, METABRIC) was performed using RStudio v1.1.3, R v3.5, samtools/ bcftools 1.8, and the R packages 'TCGAbiolinks'/'survival'/'survminer as outlined in the methods section. Gene set enrichment analysis was performed using the R package clusterProfiler v3.12. Immunofluorescent and phase contrast images, and Western blot quantification were analyzed using Fiji/ ImageJ (v2.14.0). Optically cleared tumors were analyzed using Imaris. All other graphs and statistical analyses were generated using Graphpad Prism v8. Microsoft Excel v16 was used for data processing. Flow cytometry data was collected on the Attune software and analyzed using FlowJo (v10.10.0).

For manuscripts utilizing custom algorithms or software that are central to the research but not yet described in published literature, software must be made available to editors and reviewers. We strongly encourage code deposition in a community repository (e.g. GitHub). See the Nature Portfolio guidelines for submitting code & software for further information.

Data

Policy information about availability of data

All manuscripts must include a data availability statement. This statement should provide the following information, where applicable:

- Accession codes, unique identifiers, or web links for publicly available datasets
- A description of any restrictions on data availability
- For clinical datasets or third party data, please ensure that the statement adheres to our policy

Raw sequencing data and count tables for transcriptional profiling of 4T1-derived spheroids have been deposited at the Gene Expression Omnibus under accession number GSE267958. Reads were mapped to the mouse genome assembly GRCm38. Data for the METABRIC study are publicly available under the EGA accession number EGAS00000000083; data from the TCGA study are publicly available from https://portal.gdc.cancer.gov.

Human research participants

Policy information about studies involving human research participants and Sex and Gender in Research.

Reporting on sex and gender	All human samples used in the study were from female breast cancer patients (>99% of all breast cancer cases).
Population characteristics	No data on population characteristics has been used in the manuscript.
Recruitment	Fresh and FFPE breast tumor samples were obtained from Cooperative Human Tumor Network (CHTN).
Ethics oversight	All research involving human samples at The Rockefeller University is supervised by a Institutional Review Board (IRB). All samples in this study were fully anonymized before being received at The Rockefeller University. The Rockefeller University IRB determined that our study was IRB-exempt.

Note that full information on the approval of the study protocol must also be provided in the manuscript.

Field-specific reporting

Please select the one below that is the best fit for your research. If you are not sure, read the appropriate sections before making your selection.

☒ Life sciences ☐ Behavioural & social sciences ☐ Ecological, evolutionary & environmental sciences

For a reference copy of the document with all sections, see nature.com/documents/nr-reporting-summary-flat.pdf

Life sciences study design

All studies must disclose on these points even when the disclosure is negative.

Sample size	No statistical methods were used to predetermine sample sizes. Sample sizes were arrived based on having at least three independent biological replicates.
Data exclusions	No data exclusions used.
Replication	Studies were repeated and successfully replicated at least twice (biological replicates).
Randomization	Allocation to different experiments was random. For in-vivo experiments, mice were age- and gender-matched; litter mates were used when possible and animals were randomized to each experimental cohort.
Blinding	Tumor measurements and metastasis quantification was performed in a blinded manner. Additionally, all MFI quantifications were performed in a blinded manner.

Reporting for specific materials, systems and methods

We require information from authors about some types of materials, experimental systems and methods used in many studies. Here, indicate whether each material, system or method listed is relevant to your study. If you are not sure if a list item applies to your research, read the appropriate section before selecting a response.

Materials & experimental systems

n/a	Involved in the study
☐	☒ Antibodies
☐	☒ Eukaryotic cell lines
☒	☐ Palaeontology and archaeology
☐	☒ Animals and other organisms
☐	☒ Clinical data
☒	☐ Dual use research of concern

Methods

n/a	Involved in the study
☒	☐ ChIP-seq
☐	☒ Flow cytometry
☒	☐ MRI-based neuroimaging

Antibodies

Antibodies used

Primary antibodies used for Western blotting included mouse βIII-tubulin (1:1000; Biolegend, MMS-435P, Clone TUJ1), rabbit GAPDH (1:1000; Cell Signaling 2118, 14C10), mouse HSP-60 (1:1000; Santa Cruz Biotechnology, sc-13115), and rabbit TACR1 (1:1000; ThermoFisher, PA1-32229).

Primary antibodies used for immunofluorescence experiments include rabbit anti-CGRP (1:250, Cell Signaling, mAb#14959), mouse anti-βIII-tubulin (1:200, Biolegend, MMS-435P, Clone TUJ1), rabbit anti-Ki-67 (1:250, abcam, ab15580), rabbit anti-substance P (1:200, Sigma-Aldrich, AB1566), mouse anti-neurofilament-L (1:400, Cell Signaling, #2837), mouse anti-dsRNA (1:200, Axxora, JBS-RNT-SCI-10010200) and phalloidin (1:200, ThermoFisher Scientific, A12379). Nuclei were counterstained using Hoechst (1:500, ThermoFisher Scientific, H3579). Secondary antibodies include Donkey AlexaFluor IgG (H+L) conjugates (1:200, ThermoFisher Scientific, A21206, A21202, A31573, A31572, A31571, A31570, A21208).

Validation

All antibodies used have been validated by the manufacturers to be specific to our protein of interest for use against mouse (or human) tissue. Validation data is available at each manufacturer's website by searching under the provided catalog numbers. Manufacturer validation includes assessing cells known to express or not to express the target protein and cross-referencing the expression pattern with available literature or by orthogonal validation using an antibody independent strategy. All antibodies were also used successfully in previous peer-reviewed publications. For TACR1 and TLR7, the antibody was also validated in-house in knockdown cells.

Eukaryotic cell lines

Policy information about cell lines and Sex and Gender in Research

Cell line source(s)

4T1, EO771, HEK293T, Py8119 and MDA-MB-231 cells were obtained from American Tissue Type collection (ATCC). 4T07 and 67NR cells were a generous gift from W. P. Schiemann (Case Comprehensive Cancer Center).

Authentication

No independent authentication was perfromed.

Mycoplasma contamination

All cell lines were tested for mycoplasma contamination every ~3 months. Cells used in this study were confirmed to be negative for mycoplasma.

Commonly misidentified lines
(See ICLAC register)

No commonly misidentified lines were used in this study

Animals and other research organisms

Policy information about studies involving animals; ARRIVE guidelines recommended for reporting animal research, and Sex and Gender in Research

Laboratory animals

Age and strain of all mice used in the study are described in the results and/ or methods section. All female mice were used in the study. Genetic strains used in the study include BALB/c, C57B6J, and NSG. For mammary fat pad injections and intraductal injections, 5-8 week old mice were used. 6-10 week old female mice were used for tail vein experiments. DRG neurons were isolated from 4-8 week old female mice.

Wild animals

Study did not involve wild animals

Reporting on sex

Only female mice were used in the study.

Field-collected samples

Study did not involve field-collected samples

Ethics oversight

All animal experiments were performed in accordance with the guidelines of the Institutional Animal Care and Use Committee (IACUC) at the Rockefeller University.

Note that full information on the approval of the study protocol must also be provided in the manuscript.

Clinical data

Policy information about clinical studies

All manuscripts should comply with the ICMJE guidelines for publication of clinical research and a completed CONSORT checklist must be included with all submissions.

Clinical trial registration	NA
Study protocol	NA
Data collection	NA
Outcomes	NA

Flow Cytometry

Plots

Confirm that:

☒ The axis labels state the marker and fluorochrome used (e.g. CD4-FITC).

☒ The axis scales are clearly visible. Include numbers along axes only for bottom left plot of group (a 'group' is an analysis of identical markers).

☒ All plots are contour plots with outliers or pseudocolor plots.

☒ A numerical value for number of cells or percentage (with statistics) is provided.

Methodology

Sample preparation	67NR cancer cells were washed with PBS several times and detached from culture plates using gentle pipetting (no trypsin was used). Cells were stained with TACR1 (extracellular) primary antibody and AF555 secondary antibody. Cells were then resuspended at a concentration of 2-5 x 10^6 / ml and run on the flow cytometer.
Instrument	Attune flow cytometer
Software	The Attune software was used for data collection and Flowjo software v10.10 was used for data analysis.
Cell population abundance	No cell sorting was performed.
Gating strategy	An initial gate based on basal scatter characteristics served to exclude debris followed by singlet gates based on FSC-A and FSC-H. Unstained cells were used to gate for TACR1 positivity. Gating strategy is provided in the Supplementary Information.

☒ Tick this box to confirm that a figure exemplifying the gating strategy is provided in the Supplementary Information.